(NASA-CR-168174-Vol-2) ELECTROTHERMAL THRUSTER DIAGNOSTICS. VOLUME 2: TECHNICAL (TRW, Inc., Redondo Beach, Calif.) 57 p HC A04/MF A01 CSCL 21H

N83-33943

Unclas G3/20 42023


NASA CR 168174


# ELECTROTHERMAL THRUSTER DIAGNOSTICS

## Volume II: Technical

by S. Zafran and B. Jackson

**TRW Space and Technology Group**

Prepared for

**NATIONAL AERONAUTICS AND SPACE ADMINISTRATION**

Lewis Research Center

Contract NAS 3-23265

NASA CR 168174

# ELECTROTHERMAL THRUSTER DIAGNOSTICS

## Volume II: Technical

by S. Zafran and B. Jackson

**TRW Space and Technology Group**

Prepared for

**NATIONAL AERONAUTICS AND SPACE ADMINISTRATION**

Lewis Research Center

Contract NAS 3-23265

| 1. Report No. | 2. Government Accession No. | 3. Recipient's Catalog No. |
|---|---|---|
| NASA CR 168174 | | |

| 4. Title and Subtitle | 5. Report Date |
|---|---|
| Electrothermal Thruster Diagnostics<br>Volume II: Technical | May 1983 |
| | 6. Performing Organization Code |
| 7. Author(s) | 8. Performing Organization Report No. |
| S. Zafran and B. Jackson | 39152-6012-UE-00 |
| | 10. Work Unit No. |
| 9. Performing Organization Name and Address | |
| TRW<br>Space and Technology Group<br>Redondo Beach, California 90278 | 11. Contract or Grant No.<br>NAS 3-23265 |
| | 13. Type of Report and Period Covered<br>Final Report<br>5 May 1982 - 4 March 1983 |
| 12. Sponsoring Agency Name and Address | 14. Sponsoring Agency Code |
| National Aeronautics and Space Administration<br>Lewis Research Center<br>Cleveland, Ohio 44135 | |

15. Supplementary Notes

Project Manager, Michael J. Mirtich, Space Propulsion Division, NASA-Lewis Research Center

16. Abstract

Test data taken with nitrogen, hydrogen, and ammonia propellants are presented over a wide range of operating conditions at thrust levels up to 225 mN (50 mlb). The design adaptation of a flight-qualified thruster for operation with gaseous propellant inlet is described. Post-test analysis includes evaluation of thruster performance and efficiency, and shows the effects of propellant contamination on an immersed heating element.

| 17. Key Words (Suggested by Author(s)) | 18. Distribution Statement |
|---|---|
| Spacecraft propulsion<br>Electric propulsion | Unclassified-unlimited |

| 19. Security Classif. (of this report) | 20. Security Classif. (of this page) | 21. No. of Pages | 22. Price* |
|---|---|---|---|
| Unclassified | Unclassified | | |

* For sale by the National Technical Information Service, Springfield, Virginia 22161

TABLE OF CONTENTS

## 1. INTRODUCTION

Electrothermal thrusters were successfully developed by a number of investigators in the 1960s and early 1970s (References 1 and 2). Their demonstrated performance compared favorably with earlier theoretical calculations (Reference 3). The first space operation of an electrothermal thruster took place on September 15, 1965 when a 0.187 N (0.042 lbf) resistojet was fired for 30 minutes to adjust the position of a Vela nuclear detection satellite. This device used nitrogen propellant, consumed 90 watts of electrical input power, and operated at a specific impulse of 123 seconds (Reference 4). At present, 20 HiPEHTs (High Performance Electrothermal Hydrazine Thrusters) are operational in space for performing north-south stationkeeping maneuvers on Intelsat V. Sixteen of these thrusters have been fired in space. The HiPEHT (Figure 1) is a hybrid device, using chemical energy with electrothermal augmentation to achieve close to 300 seconds $I_{sp}$ (Reference 5).

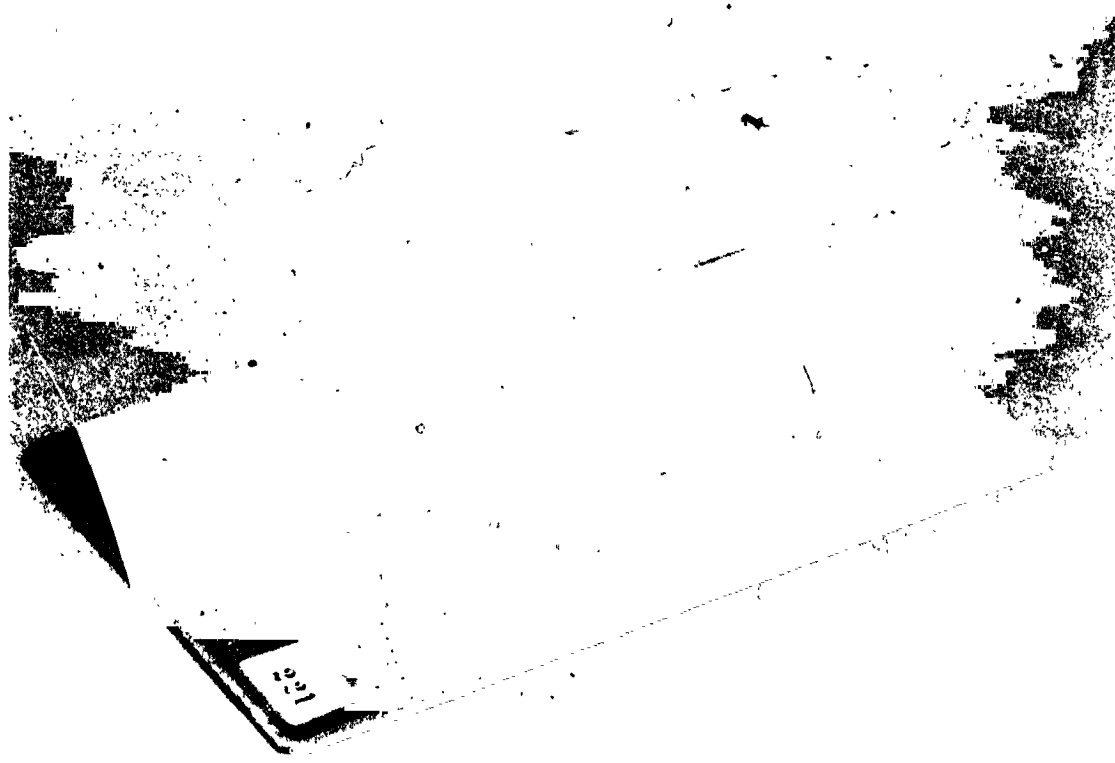

Figure 1. Flight Configuration HiPEHT Thruster

In examining onboard propulsion requirements for auxiliary propulsion of large platforms, such as Space Station, in low earth orbit, electrothermal thrusters were identified as a near-term technology with growth potential for long-term development (Reference 6). Electrothermal thrusters can be used with various propellants, including storables such as hydrazine and ammonia, with hydrogen, and with those commonly associated with manned systems, such as carbon dioxide and methane. The efflux from these thrusters is generally like the propellants, nonreactive and noncontaminating. Long-term ground tests and space operation have yielded a good data base for pursuing low risk advances in electrothermal technology.

The specific objectives of the project reported herein were to evaluate electrothermal thruster performance limitations that result from materials temperature restrictions, molecular species of exhaust propellant, and propellant/materials interactions. During the technical effort, test data were evaluated for $N_2$, $H_2$, and $NH_3$ molecular species. The augmentation heat exchanger from HiPEHT was used as the basic test article, in order to tie the test effort to a data base afforded by existing flight hardware. Earlier work along these lines involved performance characteristics of a vortex heat exchanger with nitrogen, ammonia, methane, and carbon dioxide propellants. Results from the earlier work are discussed in Reference 7, which was primarily directed towards biowaste gas applications.

The theoretical performance of the propellants tested on this project is shown as a function of gas temperature in Figure 2. Theoretical specific impulse for an ideal isentropic expansion to zero pressure is a function only of the stagnation enthalpy of the propellant. Expansion to zero pressure implies a nozzle of infinite area ratio ($\varepsilon = \infty$). Frozen flow losses (see References 1 and 3) were neglected in calculating theoretical limits.

The theoretical curve for ammonia in Figure 2 assumes full ammonia dissociation ($\alpha = 1.0$) such that the superheated gas consists only of nitrogen and hydrogen. The effects of dissociation fraction on theoretical performance with ammonia propellant are shown in Figure 3.

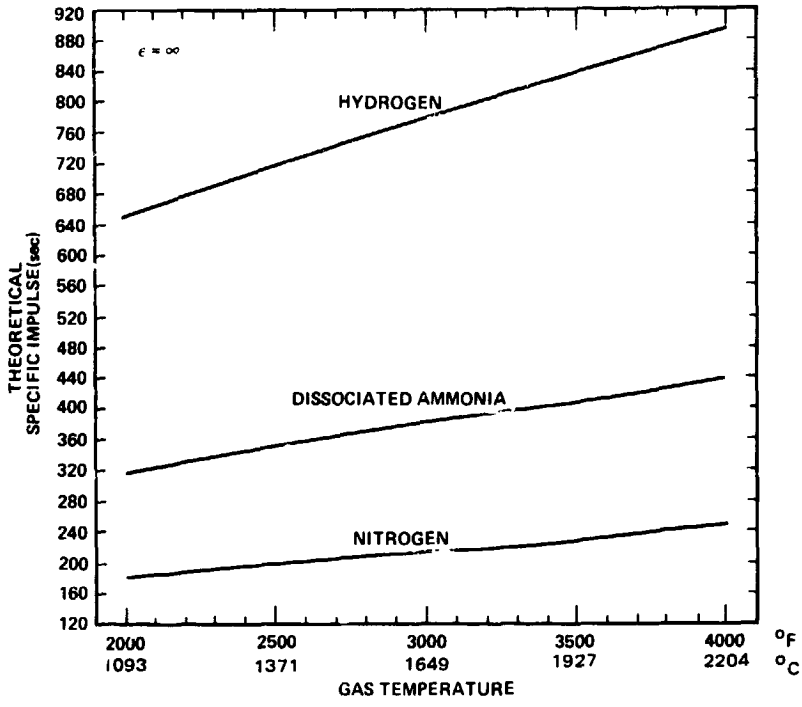


Figure 2. Specific Impulse Versus Temperature for $N_2$, $H_2$, and $NH_3$

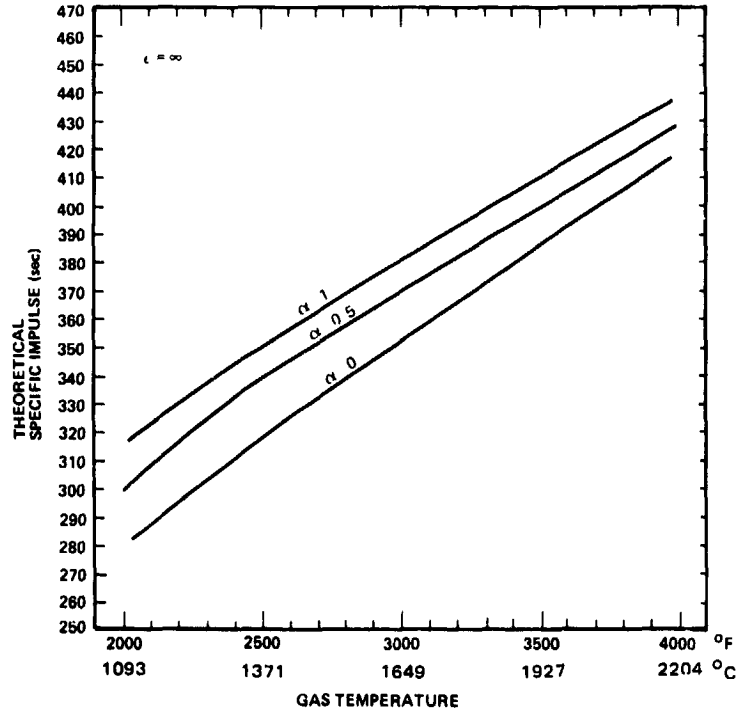


Figure 3. Specific Impulse Versus Temperature for Ammonia

## 2. ELECTROTHERMAL TEST UNIT

The test units used during this project were fabricated by modifiying the HiPEHT augmentation heat exchanger to accept gaseous, rather than liquid, propellant inlet. Figure 4 is a photograph of an electrothermal test unit. In order to understand how this unit evolved from HiPEHT, the following discussion will first describe the HiPEHT thruster, and will then identify the hardware that was used in the test unit.

The HiPEHT thruster configuration is shown isometrically in Figure 5, and in cross-section in the line drawing of Figure 6. The thruster contains two major sections: a propellant decomposition chamber and a high temperature heat exchanger. As in a standard monopropellant thruster, liquid hydrazine controlled by a propellant valve is fed through an injector feed tube into a decomposition chamber. There it vaporizes and decomposes to produce a hot gas mixture of nitrogen, hydrogen, and ammonia at temperatures in the range of $870^{o}$ to $980^{o}$C ($1600^{o}$ to $1800^{o}$F). In a conventional thruster, the thermal energy of the gas is then converted to kinetic energy by expulsion through the exhaust nozzle, thereby producing a reactive thrust. In HiPEHT, an intermediate heat exchanger is used to increase the gas temperature to $1650^{o}$ to $1930^{o}$C ($3000^{o}$ to $3500^{o}$F) prior to expulsion. Since specific impulse varies with the square root of absolute gas temperature, this temperature increase represents an approximate 30 to 40 percent increase in performance. The heat exchanger augments the gas mixture energy via an electrically powered, close-coupled resistance heater. The augmented thruster specific impulse is ideally limited only by the final gas temperature. In reality, lower limits exist because of maximum temperature restrictions on the heat exchanger materials.

Theoretical and demonstrated thruster performance with hydrazine propellant, in terms of specific impulse and specific power as functions of gas temperature, are shown in Figure 7. The theoretical curves assume full ammonia dissociation ($\alpha$ = 1.0), such that the super-heated gas consists only of nitrogen and hydrogen. Note that the actual ammonia dissociation fraction is calculated to be about 80 percent. Since dissociation is an endothermic process, the actual specific power can be either less than or greater than theoretical for complete dissociation, depending on

Figure 4. Electrothermal Test Unit

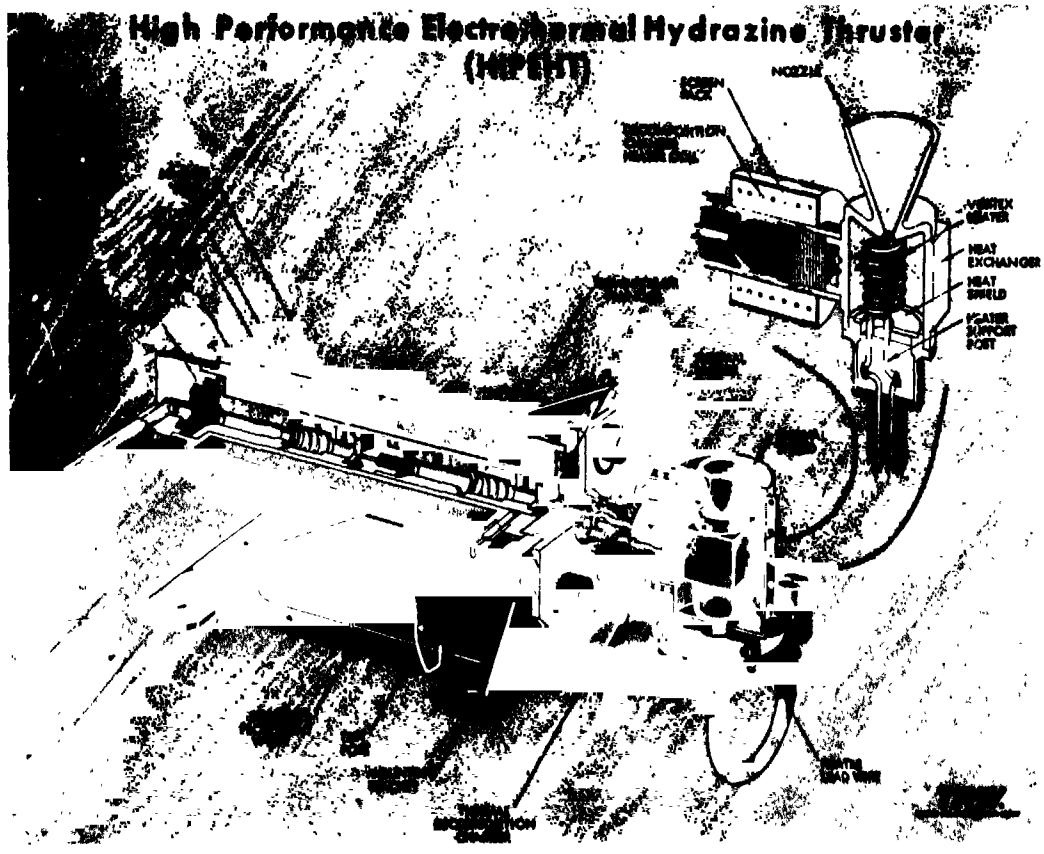


Figure 5. HiPEHT Isometric Representation

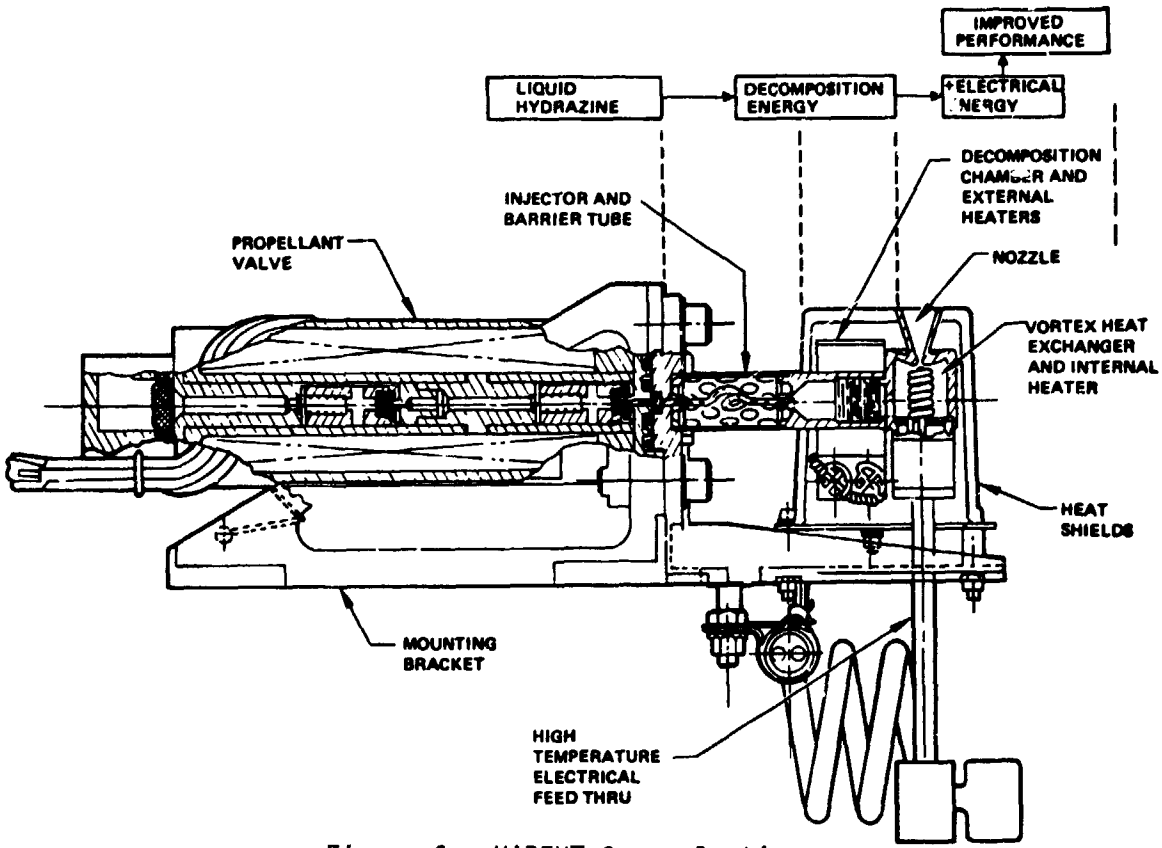


Figure 6. HiPEHT Cross Section

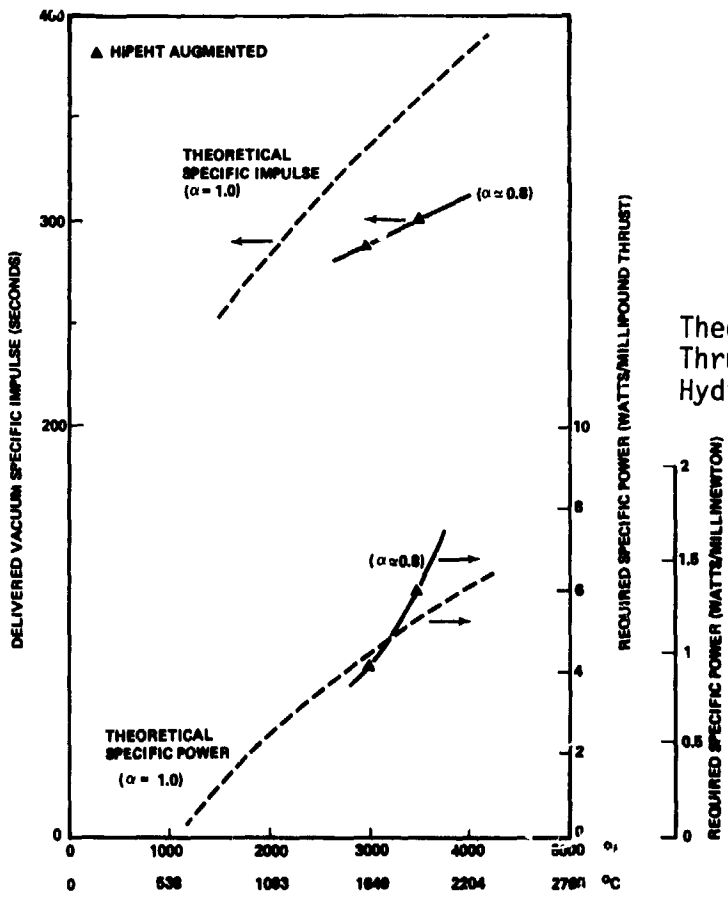


Figure 7

Theoretical and Demonstrated Thruster Performance with Hydrazine Propellant

the heat losses. In terms of specific impulse, demonstrated performance is approximately 85 percent efficient. In terms of power input to the thruster versus power transferred to gases for dissociation or as sensible heat, it is about 90 percent efficient (Reference 5). Appendix A provides additional HiPEHT performance data.

In a well designed vortex heat exchanger, propellant temperature will closely approach the temperature of the heater element prior to expulsion through the nozzle. This is accomplished by placing the heater element in a flow field where the radial and axial velocities are much smaller than the tangential velocities. Consequently, high gas velocities across the heater surface are maintained while residence times of the gases contacting the heater are extended; both factors increase heat exchange efficiency. In addition, external heat losses are minimized by the regenerative effect provided by the relatively cooler gases swirling on the outside and spiraling inward as well as by the small size of the overall heat exchanger.

The heater element (Figure 8) employed in the heat exchanger has a double helix wire (coiled-coil) configuration located along the axis of a cylindrical cavity. Propellant gases are injected tangentially into the

Figure 8. Vortex Heater Element

cavity to establish a vortex flow field. These gases spiral radially inward toward the heater element. High temperature exhaust gases leave the heat exchanger axially through a nozzle located at one end of the cavity. A high temperature electrical feedthrough at the closed cavity end affords the electrical interface between the vortex heater element and spacecraft wiring. The feedthrough thermal design achieves the proper thermal conduction and radiation balance to control heat transfer to the spacecraft, minimize ohmic heating losses and maintain the wire temperature safely below its material design limits.

The drawing in Figure 9 identifies the usable HiPEHT hardware that was employed during diagnostic testing. In summary, its vortex heat exchanger, including the heater element and electrical leads, were used. A molybdenum-rhenium (Mo-Re) adapter was designed for fitting on the upstream side to the nozzle body. The adapter was nominally 0.64 cm (1/4-in) diameter, to which a 0.32 cm (1/8-inch) OD Mo-Re tube was brazed. The adapter, similarly, was welded to the nozzle body. Two basic thruster test units of identical design were fabricated for testing.

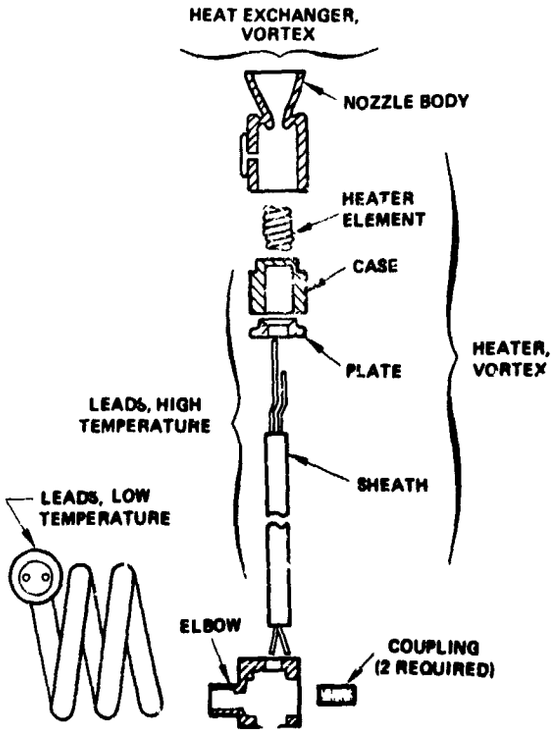


Figure 9. Usable HiPEHT Hardware

On the upstream side of the thruster assembly, the Mo-Re tubing was attached to 0.32 cm (1/8-inch) OD stainless steel tubing via mechanical coupling. This allowed for rapid hookups and disconnections between the thruster assembly and fixed propellant feed system, instrumentation, and hardware.

## 3. TEST SETUP

The test facility was set up in accordance with the schematic diagram shown in Figure 10. The thruster test unit was mounted on a thrust stand inside the vacuum test chamber. Inlet pressure to its vortex heat exchanger was measured by a pressure transducer downstream of the manually actuated firing valve. Ammonia mass flow was measured by a mass flowmeter which operates on a thermal principle of flow measurement. Its flow sensing element is in line with an optional calibrated orifice arrangement, which could also be used (or bypassed) for flow measurement. Calibrated orifices were employed for nitrogen and hydrogen mass flow measurements. A pressure gage at the inlet to the mass flowmeter provided for more accurate data reduction based on flowmeter calibration characteristics.

Propellant gases were stored in pressurized cylinders and were admitted, as required, through a series of regulators and valves. Ammonia propellant was introduced through a constant temperature bath heat exchanger to assure complete ammonia vaporization. The nitrogen cylinder was also used to purge propellant lines following a test run. A gaseous nitrogen supply on the facility was employed to repressurize the vacuum chamber to atmosphere following a test run.

Figure 11 shows photographs of the vacuum test chambers at TRW's Building M-1 in Space Park. Figure 12 shows the associated test facility instrumentation.

The principal test parameters of interest are listed in Table 1. Thrust was measured directly on the thrust stand. Mass flow was measured via calibrated orifices for nitrogen and hydrogen propellants, and by the thermal flow sensor for ammonia propellant. Specific impulse was calculated from thrust and mass flow measurements. The vortex heater power was calculated from heater input voltage and current measurements. Similarly, the heater resistance was derived from these measurements. Thruster efficiency was calculated from thrust, mass flow, power, and propellant properties data (see Section 4 for efficiency definitions). The vortex heater element temperature was determined from its resistance data and

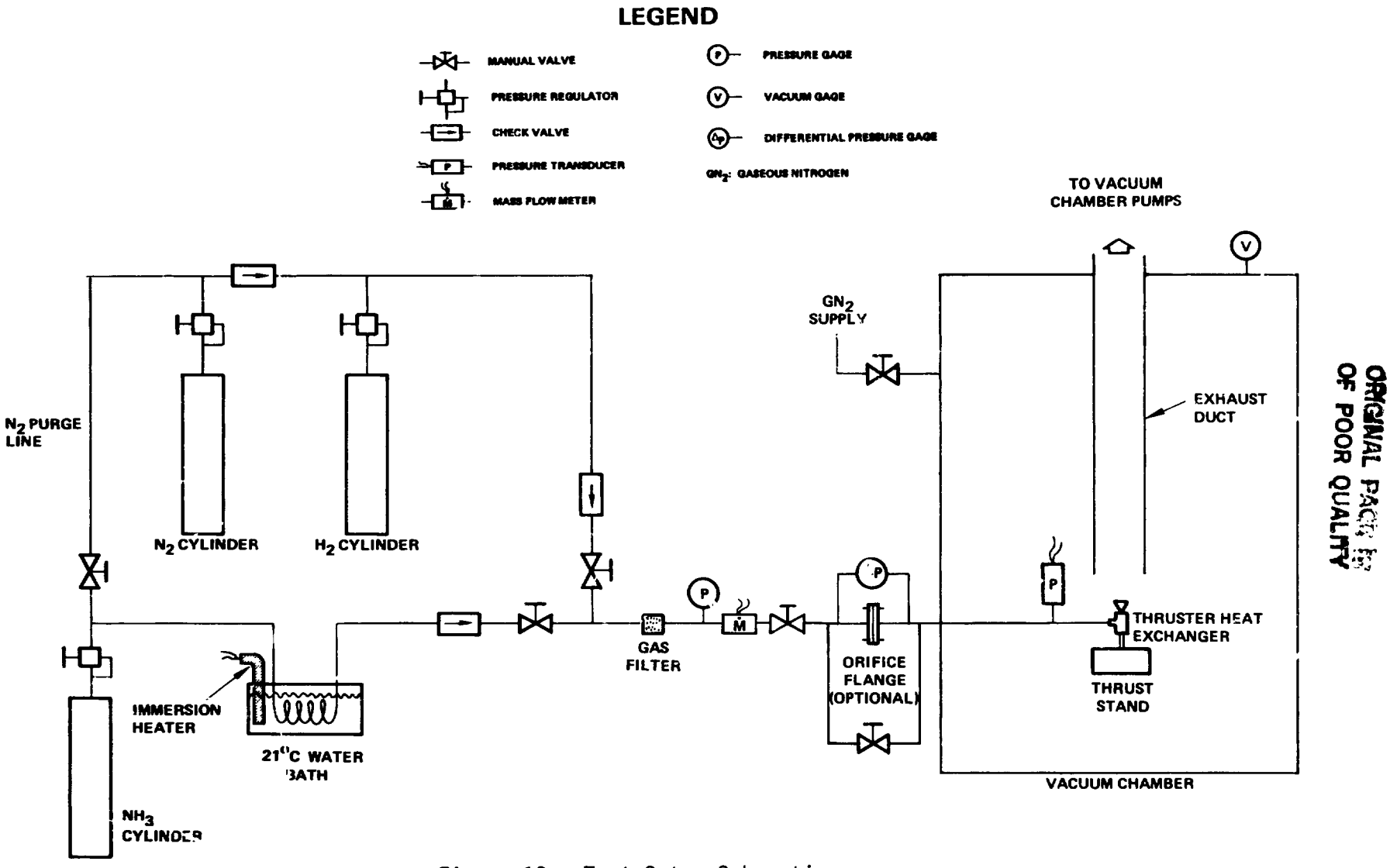


Figure 10. Test Setup Schematic

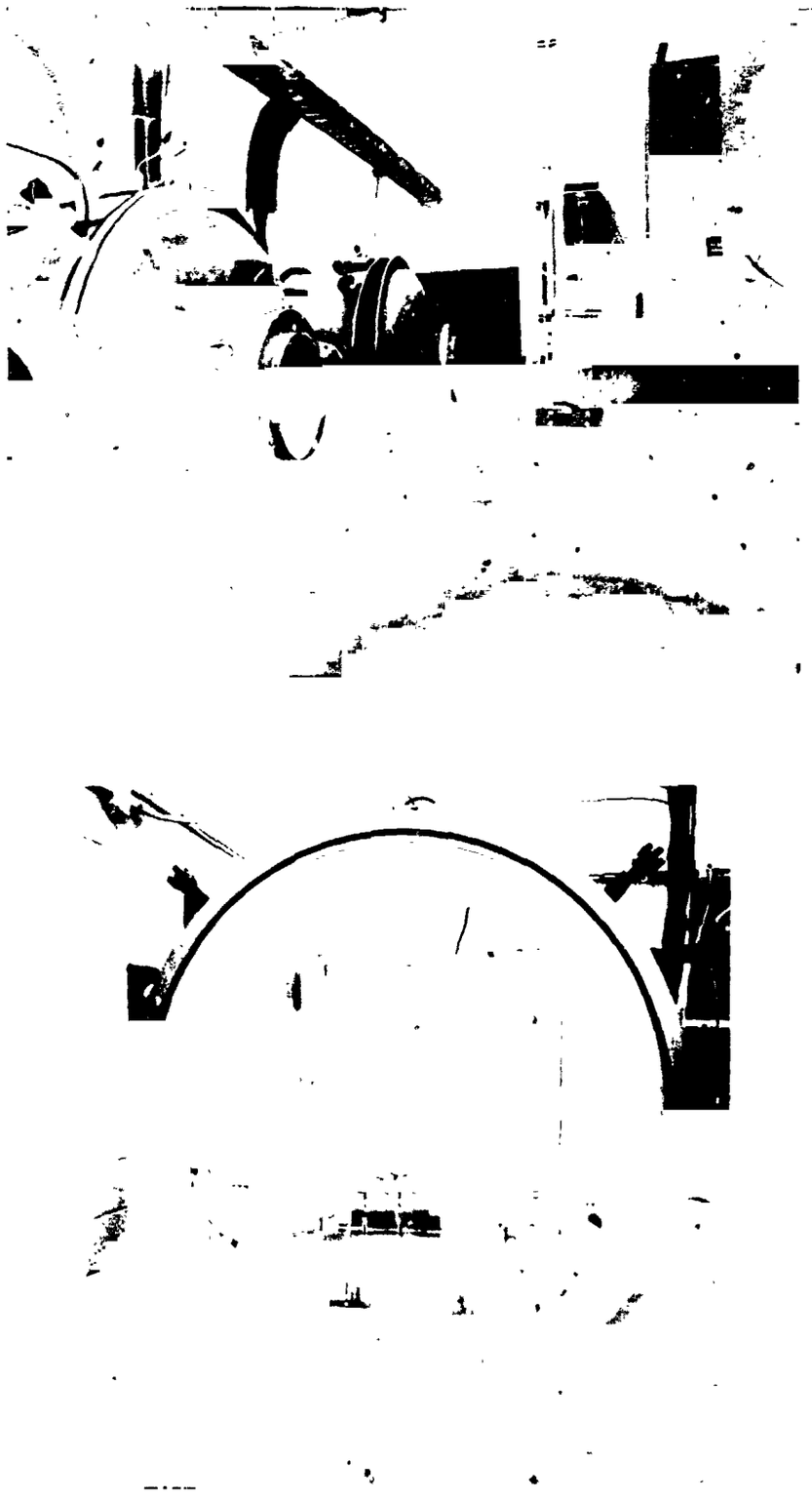

Figure 11. Vacuum Chambers

Figure 12. Data Acquisition Equipment

Table 1. Principal Test Parameters

| Parameter | Measured | Derived | Remarks |
|---|---|---|---|
| Thrust | X | | Direct Thrust Stand Measurement |
| Mass Flow | X | | Thermal Flow Sensor/Orifice |
| Specific Impulse | | X | |
| Vortex Heater Power | | X | From I - V Measurements |
| Voltage (V) | X | | |
| Current (I) | X | | |
| Resistance | | X | From I - V Measurements |
| Efficiency | | X | |
| Vortex Heater Element Temperature | | X | From Heater Resistance Measurement |
| Gas Temperature | | X | From Enthalpy Balance |
| Heat Exchanger Inlet Pressure | X | | |
| Heat Exchanger Wall Temperature | X | | |
| Propellant Inlet Temperature | X | | |
| Vacuum Chamber Pressure | X | | |

prior bell jar calibration of a vortex heater element under no flow conditions. Exit gas temperature was determined from an enthalpy balance calculation. Other measurements included thruster (heat exchanger) inlet pressure, heat exchanger wall temperature, propellant inlet temperature, and vacuum chamber pressure.

# 4. TEST DATA

Cold flow and hot firing test data were obtained with nitrogen, hydrogen, and ammonia propellants. The test data are summarized in Appendixes B, C, D and this section of the report.

## 4.1 NITROGEN PROPELLANT

Nitrogen cold flow specific impulse ranged from 74 to 77 seconds compared with a theoretical value of 80 seconds at 21°C (70°F). These data were taken at flow rates from 0.13 to 0.06 gm/sec (2.85 to 1.25 x $10^{-4}$ lb/sec). The vacuum chamber pressure measured between 0.9 and 1.5 torr during the nitrogen tests, including cold flow and hot firing.*

Nitrogen performance data are summarized in Figure 13, where specific impulse is shown as a function of power-to-thrust ratio. The solid line on this figure follows the relationship

$$I_{sp} = 80 + 20\ (P/F) \qquad (1)$$

where

$I_{sp}$ = specific impulse (sec)

P = IV = electrical input power (watts)

F = thrust (mlbf)

I = heater current (amperes)

V = heater voltage (volts)

Note that this relationship yields a cold flow (i.e., zero power) $I_{sp}$ of 80 seconds.

*Subsequent tests conducted at 0.13 gm/sec (2.85 x $10^{-4}$ lb/sec) flow and a vacuum chamber pressure of 0.2 torr yielded similar results to those reported herein.

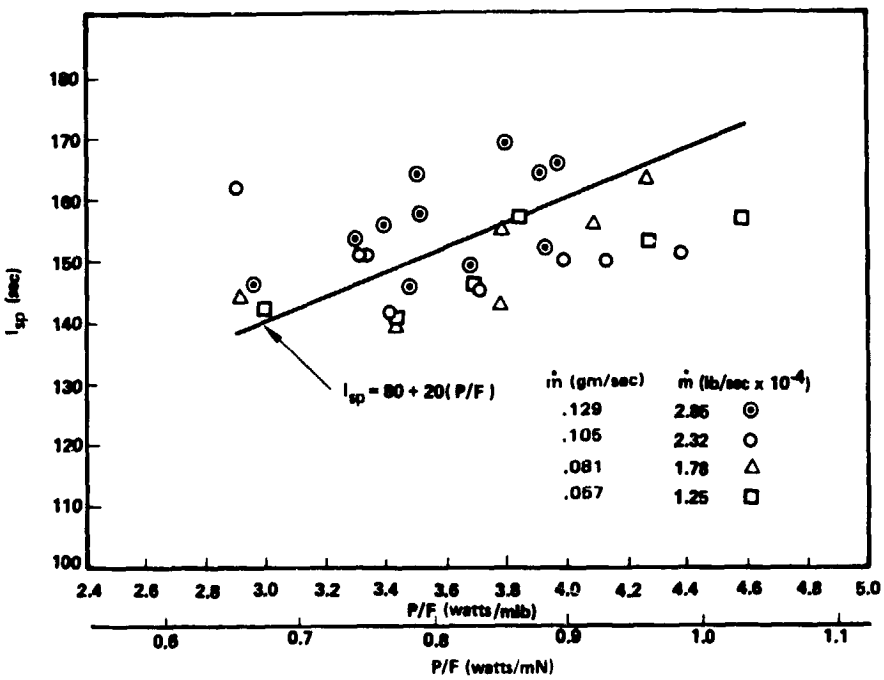


Figure 13. Nitrogen Performance

Overall efficiency as a function of specific impulse is shown in Figure 14 for five different mass flow rates. Overall efficiency is defined by (Reference 8):

$$\eta^* = 21.8 \times 10^{-3} \frac{FI_{sp}}{P_{in}} \qquad (2)$$

$$= 21.8 \times 10^{-3} \frac{FI_{sp}}{(IV + \dot{m}h)} \qquad (3)$$

where

$\eta^*$ = overall efficiency

$\dot{m}$ = propellant mass flow (gm/sec)

h = enthalpy of propellant at inlet conditions (J/gm)

$P_{in}$ = electrical plus chemical power supplied to the thruster (watts)

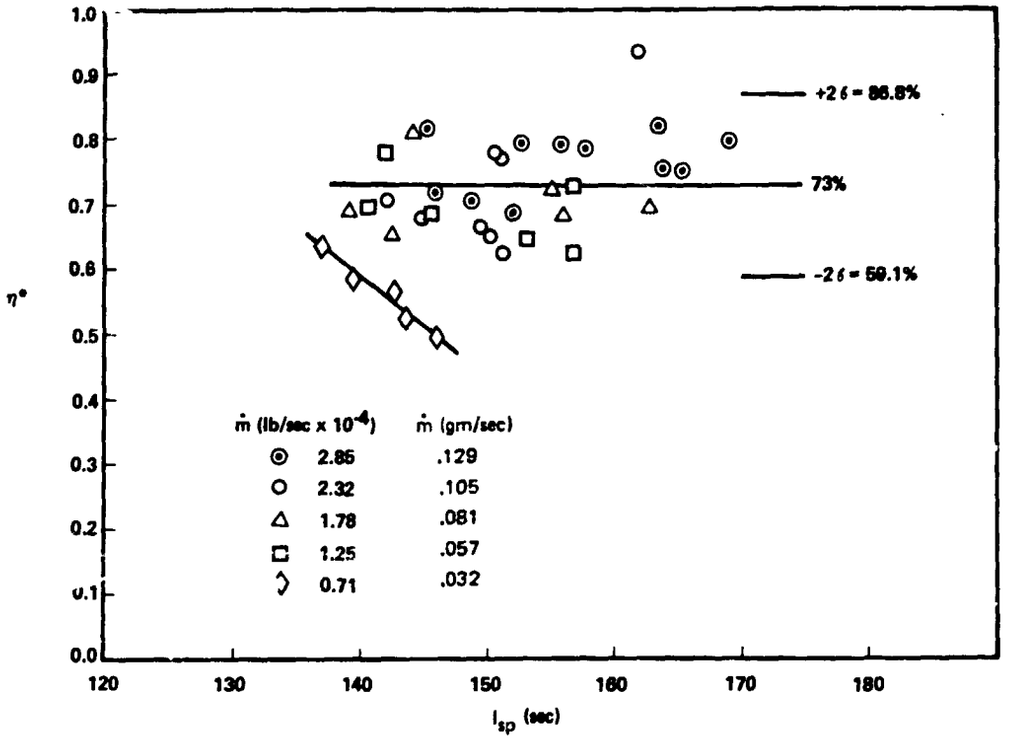


Figure 14. Nitrogen Overall Efficiency

The low flow rate data show a sharp reduction in overall efficiency with increasing specific impulse. This is because of either flow separation, viscous losses in the low-Reynolds-number nozzle (Reference 9) or poor heat transfer in a low-density vortex flow field. The low flow rate data were deliberately omitted from Figure 13 because they were not representative of nitrogen performance. The remaining data indicate 73 percent overall efficiency. The ±13.9 percent 2 $\sigma$ limits are shown in Figure 14.

Performance data as a function of mass flow are shown graphically in Figures 15(a) through 15(d). These data were taken at a vortex heater element temperature of approximately 2090°C (3800°F). The element temperature was determined from a prior calibration of typical element resistance versus optical pyrometer reading in vacuum (no flow conditions), taking lead wire resistance into account.

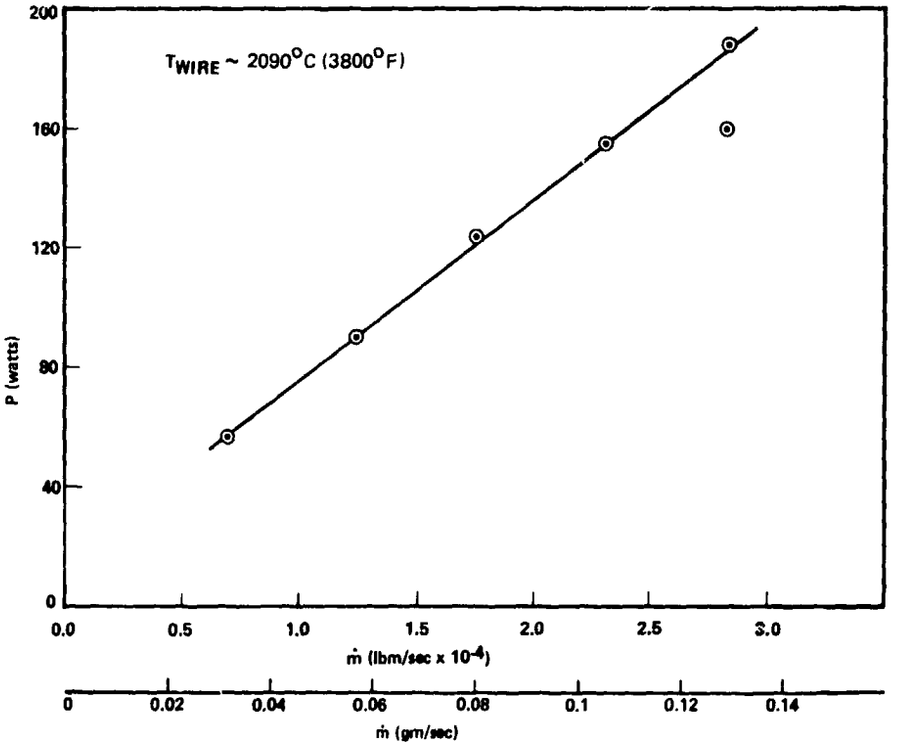


(a)

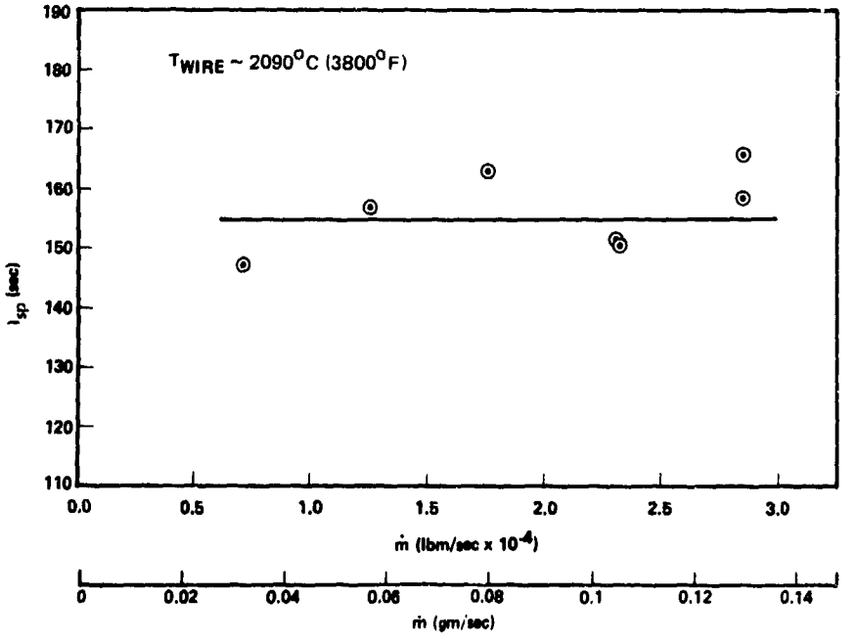


(b)

Figure 15. Performance Versus Mass Flow, Nitrogen Propellant, ∿2090°C (3800°F) Heater Temperature

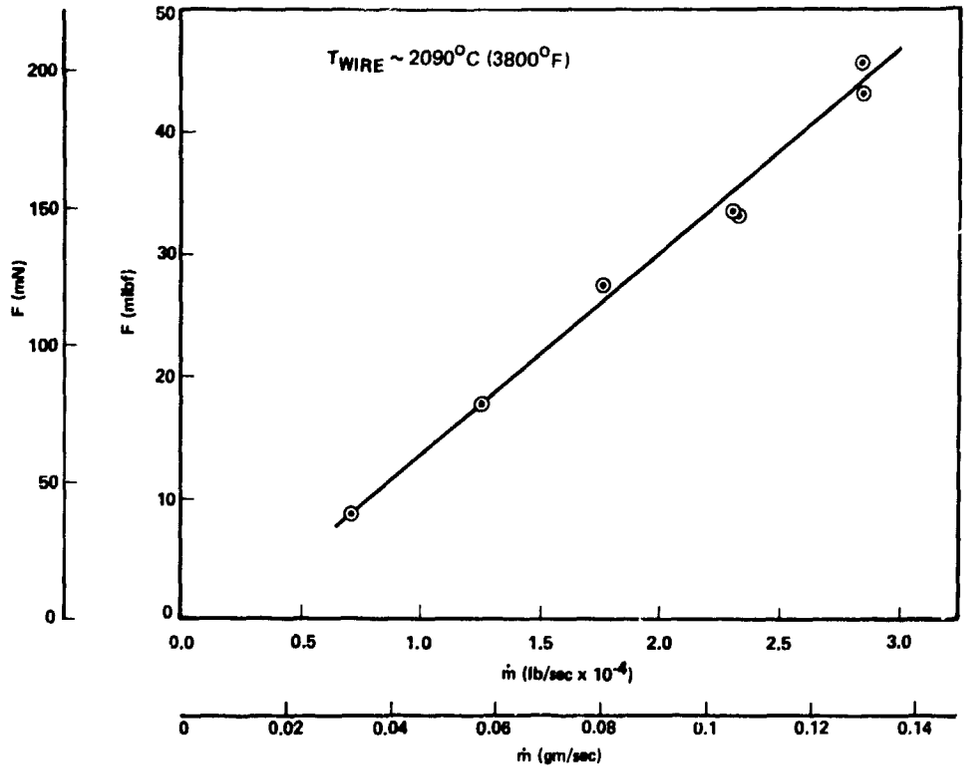


(c)

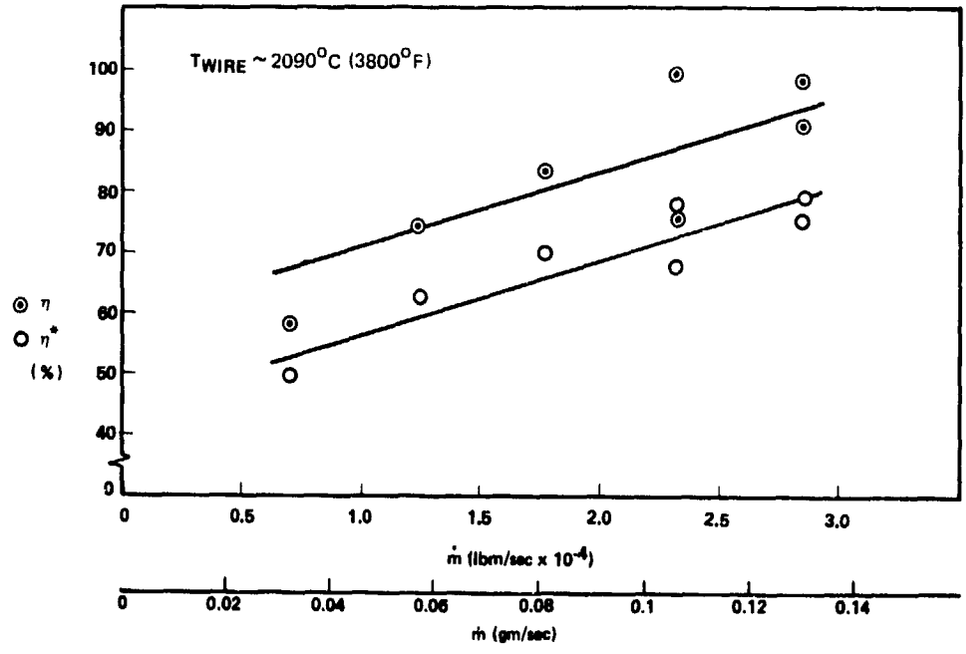


(d)

Figure 15. Performance Versus Mass Flow, Nitrogen Propellant, ∿2090°C (3800°F) Heater Temperature (Continued)

In Figure 15(d), both electrical efficiency and overall efficiency are plotted versus mass flow. Electrical efficiency is defined by:

$$\eta = 21.8 \times 10^{-3} \frac{FI_{sp}}{IV} \tag{4}$$

$$= 21.8 \times 10^{-3} \frac{I_{sp}}{(P/F)} \tag{4a}$$

where only electrical input power is used in the denominator. Overall efficiency, as defined earlier, includes chemical power as well.

Figure 16 presents thrust as a function of vortex heat exchanger injection pressure for five flow rates. The data in Figures 13, 14, and 16 were taken at heater element temperatures ranging from 1650° to 2090°C (3000° to 3800°F).

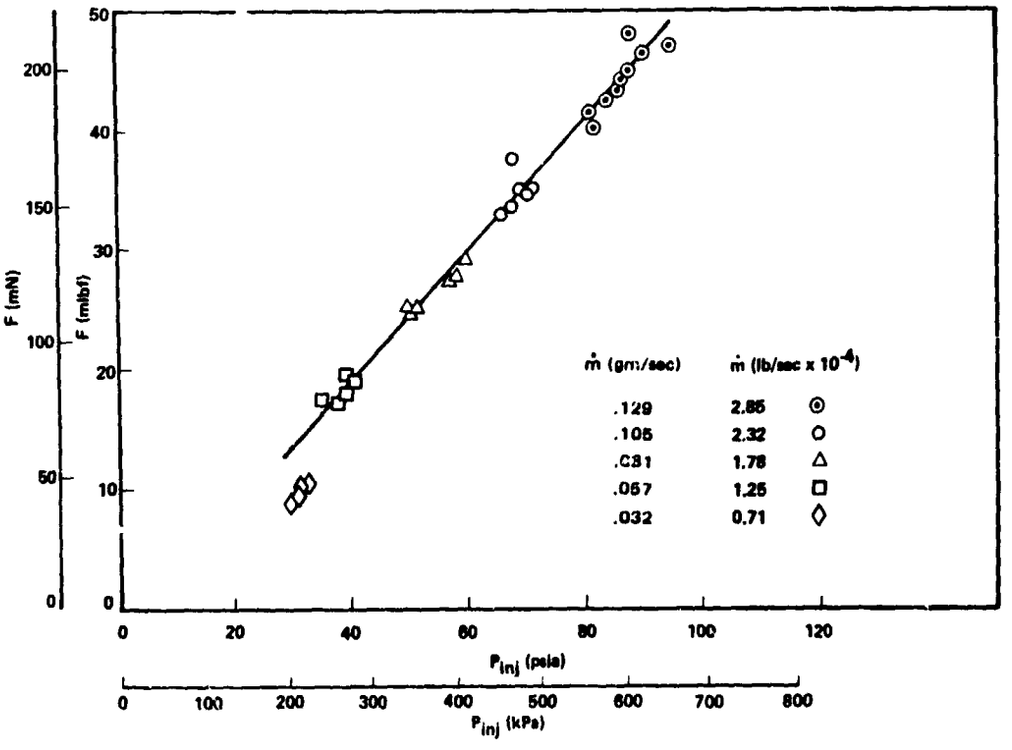


Figure 16. Thrust Versus Injection Pressure

## 4.2 HYDROGEN PROPELLANT

The hydrogen test data were taken at vacuum chamber pressures below 0.4 torr. Cold flow specific impulse ranged from 250 to 259 seconds compared with a theoretical value of 294 seconds. These data were taken at flow rates from 0.027 to 0.012 gm/sec (0.60 to 0.26 x $10^{-4}$ lb/sec). At the lowest flow rate of 0.007 gm/sec (0.15 x $10^{-4}$ lb/sec), cold flow specific impulse measured only 233 seconds, indicating possible flow separation.

Hydrogen performance data are summarized in Figure 17, where specific impulse is shown as a function of power-to-thrust ratio. The solid line in this figure follows the relationship

$$I_{sp} = 294 + 15\ (P/F) \qquad (5)$$

This relationship yields a cold flow (i.e., zero power) $I_{sp}$ of 294 seconds, corresponding to the theoretical cold flow specific impulse for hydrogen at 21°C (70°F).

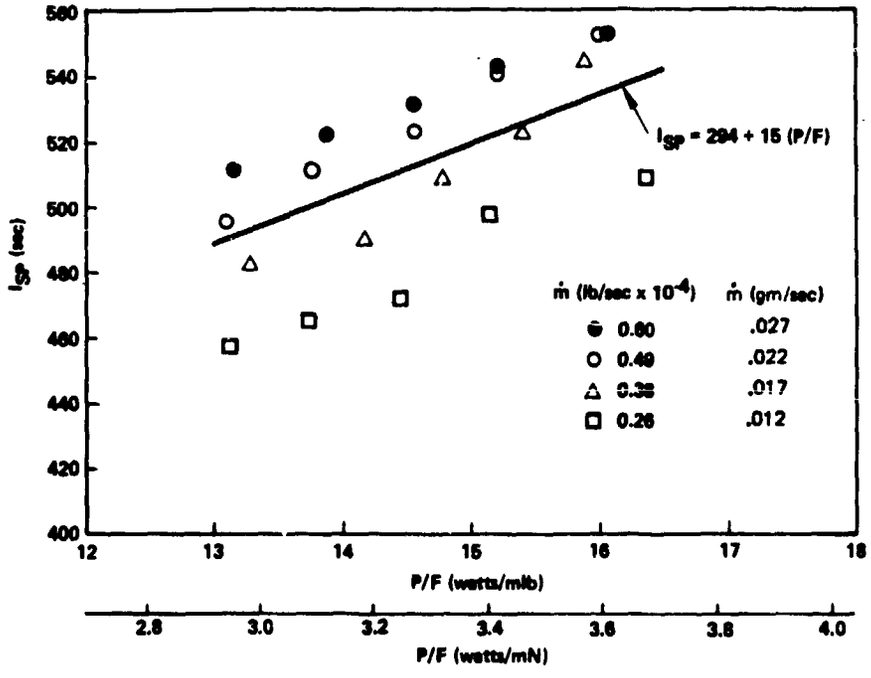


Figure 17. Hydrogen Performance

Overall efficiency as a function of specific impulse is shown in Figure 18 for five different mass flow rates. As previously experienced for nitrogen, the low mass flow rate data show a sharp reduction in overall efficiency with increasing specific impulse. This is because of either flow separation, viscous losses in the low-Reynolds-number nozzle or poor heat transfer in a low-density vortex flow field. The low flow rate data were deliberately omitted from Figure 17 because they were not representative of hydrogen performance. The remaining data indicate 61 percent overall efficiency. The ±6.1 percent 2 σ limits are shown in Figure 18.

Performance data as a function of mass flow rate are shown in Figures 19a through 19d. These data were taken at a vortex heater element temperature of approximately 2090°C (3800°F).

Figure 20 presents thrust as a function of vortex heat exchanger injection pressure for five flow rates. The data in Figures 17, 18, and 20 were taken at heater element temperatures ranging from 1650° to 2090°C (3000° to 3800°F).

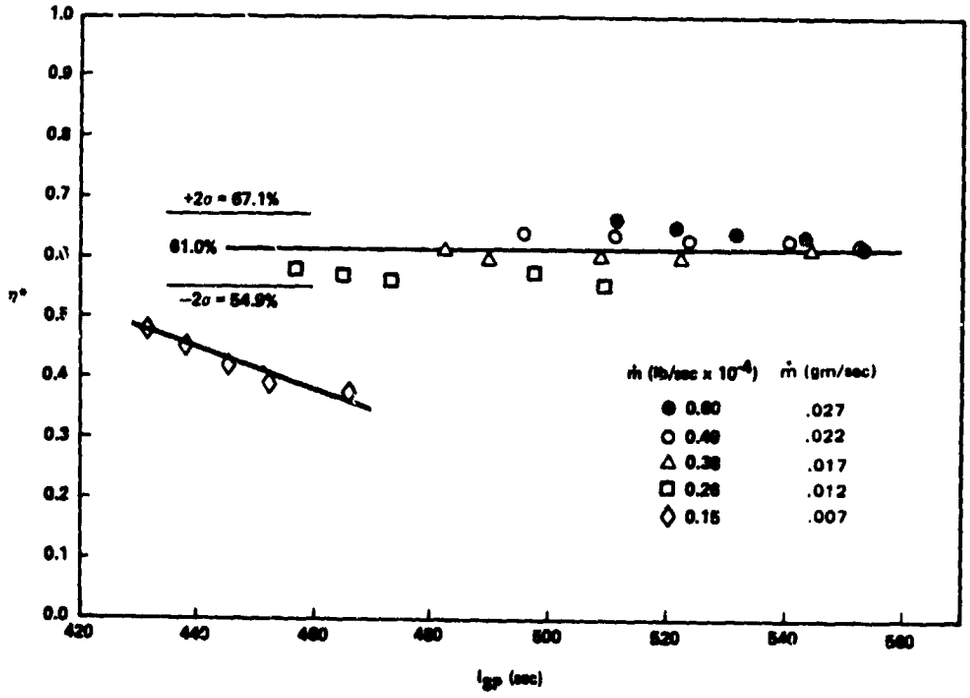


Figure 18. Hydrogen Overall Efficiency

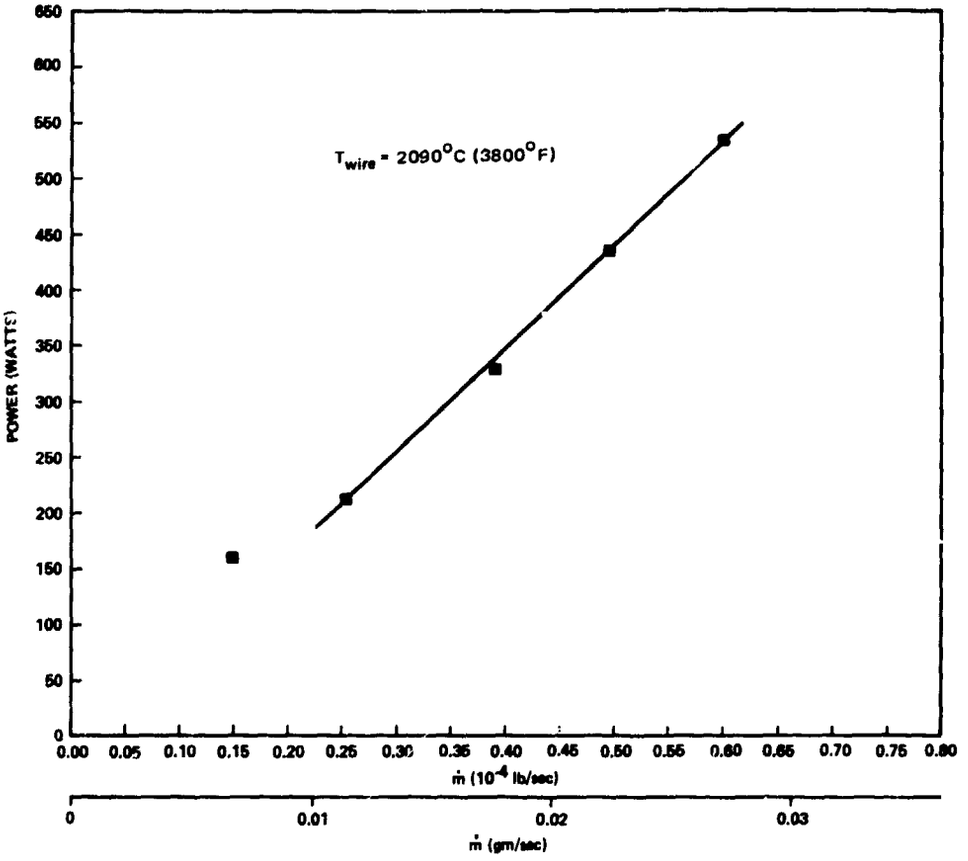


(a)

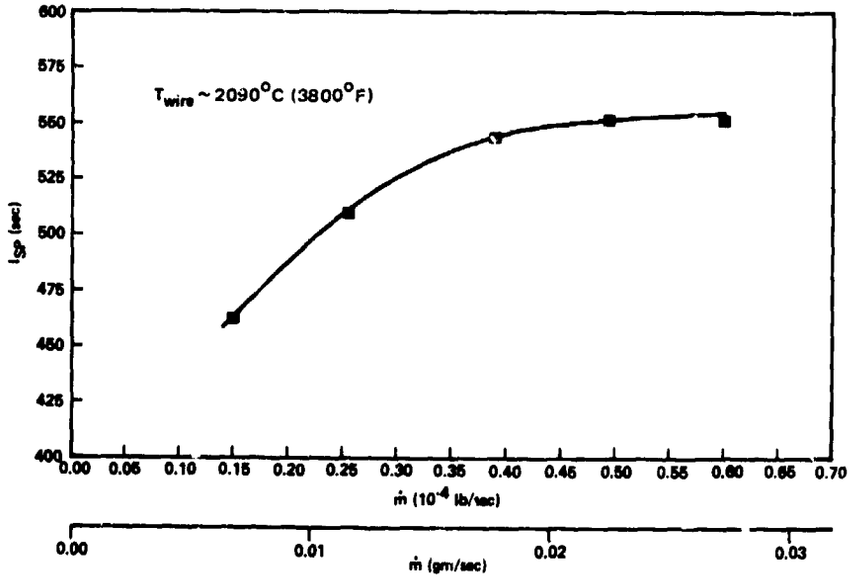


(b)

Figure 19. Performance Versus Mass Flow, Hydrogen Propellant, ~2090°C (3800°F) Heater Temperature

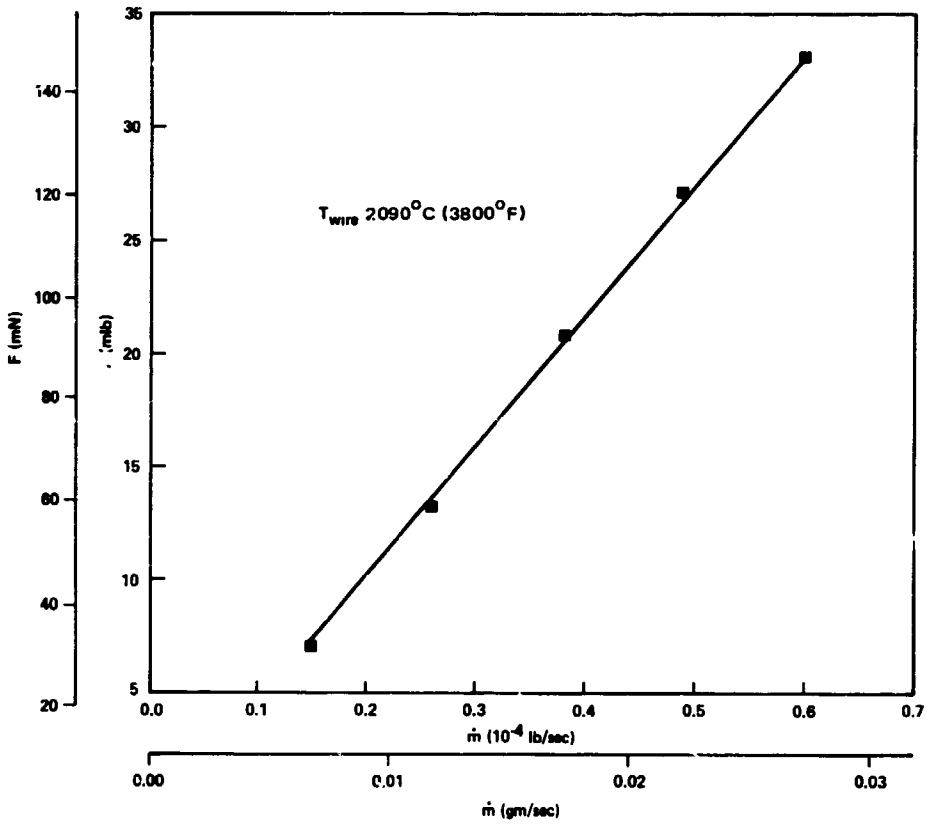


(c)

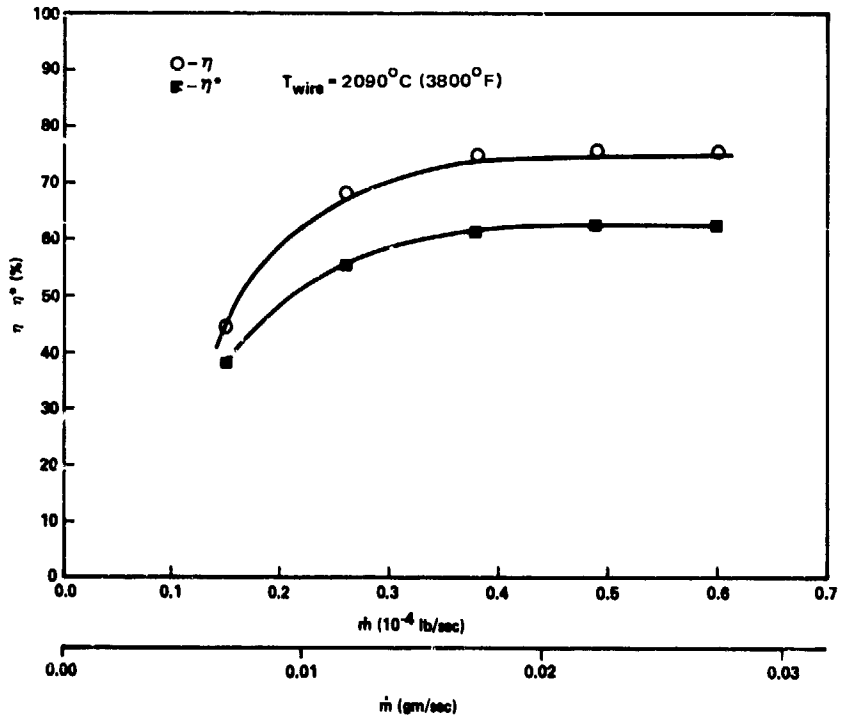


(d)

Figure 19. Performance Versus Mass Flow, Hydrogen Propellant, ∿2090°C (3800°F) Heater Temperature (Continued)

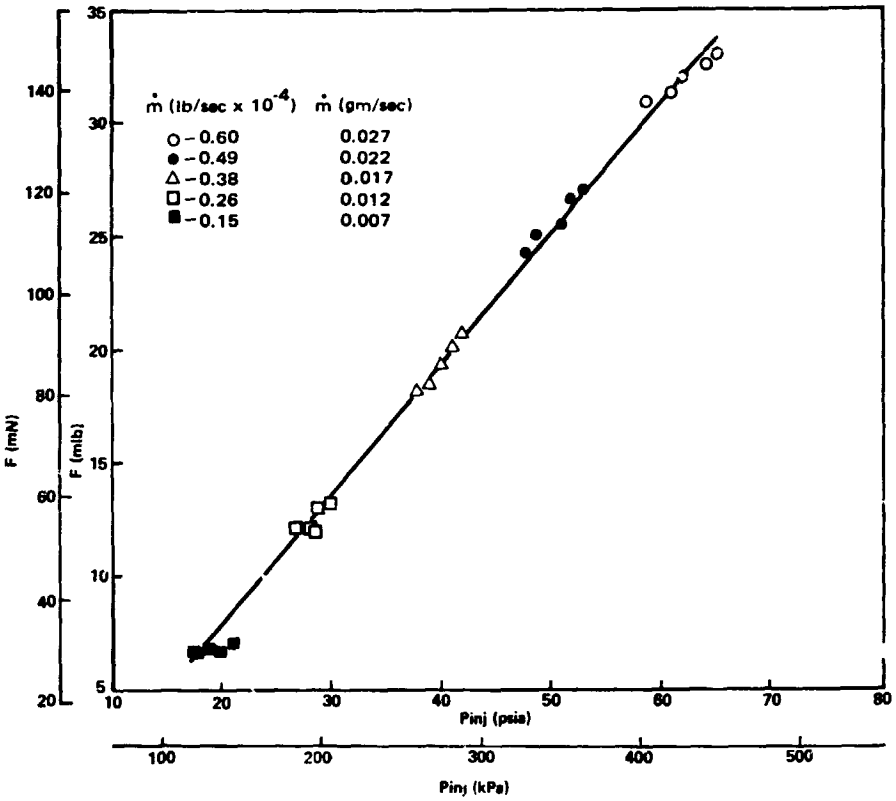


Figure 20. Thrust Versus Injection Pressure, Hydrogen Propellant

## 4.3 AMMONIA PROPELLANT

The ammonia test data were taken at vacuum chamber pressures below 0.3 torr. Cold flow specific impulse ranged from 102 to 110 seconds compared with a theoretical value of 110 seconds at 21°C (70°F).

Ammonia performance data are summarized in Figure 21. The solid line in this figure follows the relationship

$$I_{sp} = 110 + 15\ (P/F) \qquad (6)$$

This relationship yields the theoretical cold flow specific impulse of 110 seconds for ammonia at zero input power.

Overall efficiency for ammonia as a function of specific impulse is shown in Figure 22 for five different mass flow rates. Again, there is a sharp decrease in efficiency at the low mass flow rate with increasing specific impulse. Accordingly, the low flow rate data were omitted from

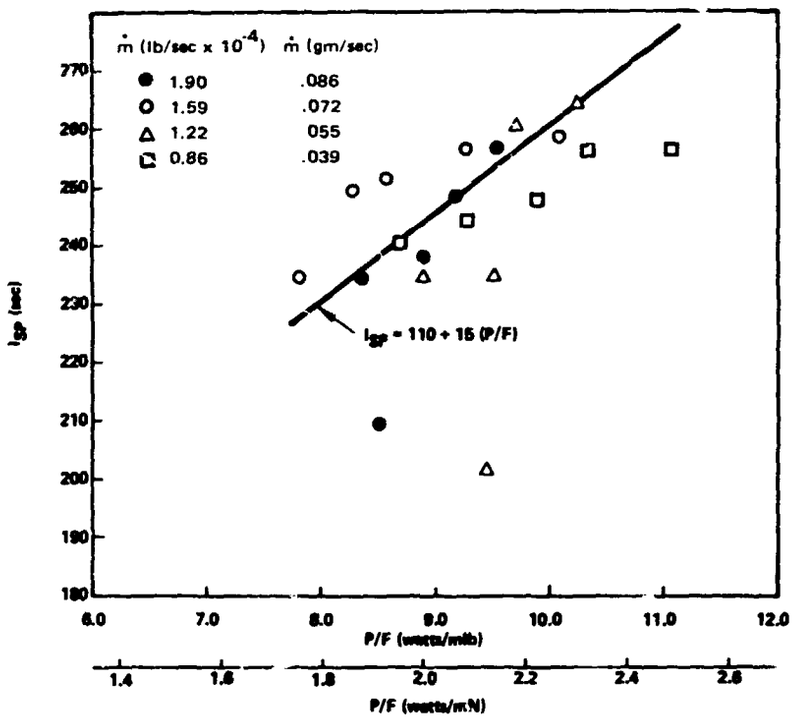


Figure 21. Ammonia Performance

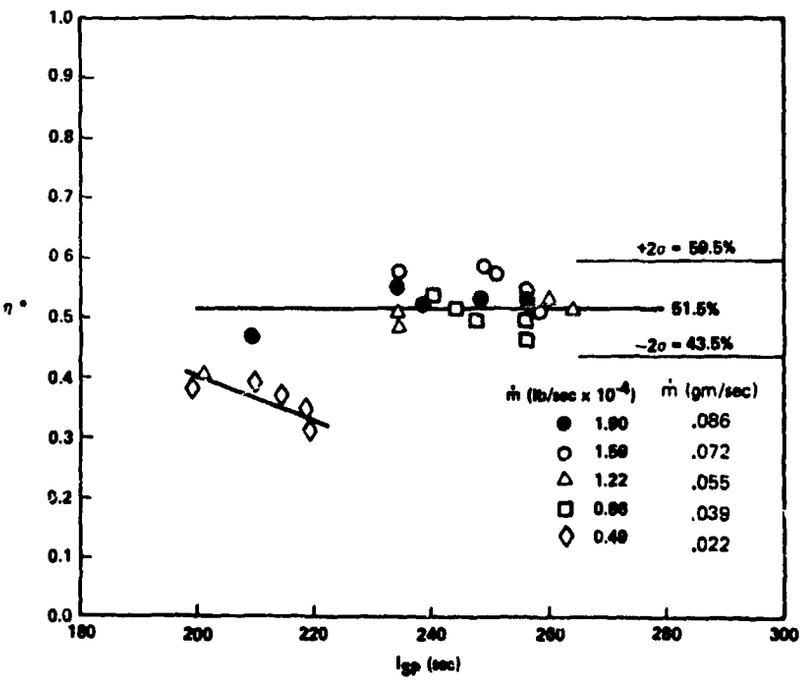


Figure 22. Ammonia Overall Efficiency

Figure 21. The remaining data indicate 51.5 percent overall efficiency. The ±8.0 percent 2 σ limits are shown in Figure 22. The lower efficiency for ammonia (than for nitrogen or hydrogen) reflects the heat of dissociation required for this propellant.

Performance data for ammonia as a function of mass flow rate are shown in Figures 23(a) through 23(d). These data were taken at a vortex heater element temperature of approximately 2090°C (3800°F). Figure 24 presents thrust versus injection pressure for five flow rates. The data in Figures 21, 22, and 24 were taken at heater element temperatures ranging from 1650° to 2090°C (3000° to 3800°F).

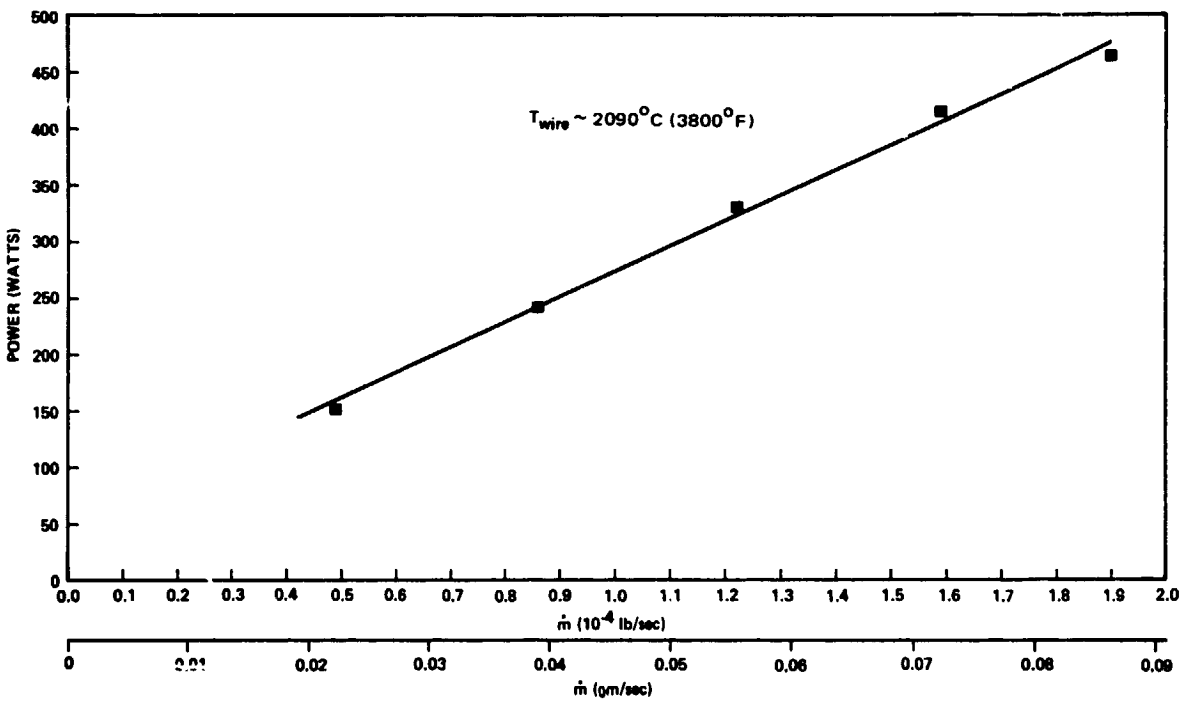


(a)

Figure 23. Performance Versus Mass Flow, Ammonia Propellant, ~2090°C (3800°F) Heater Temperature

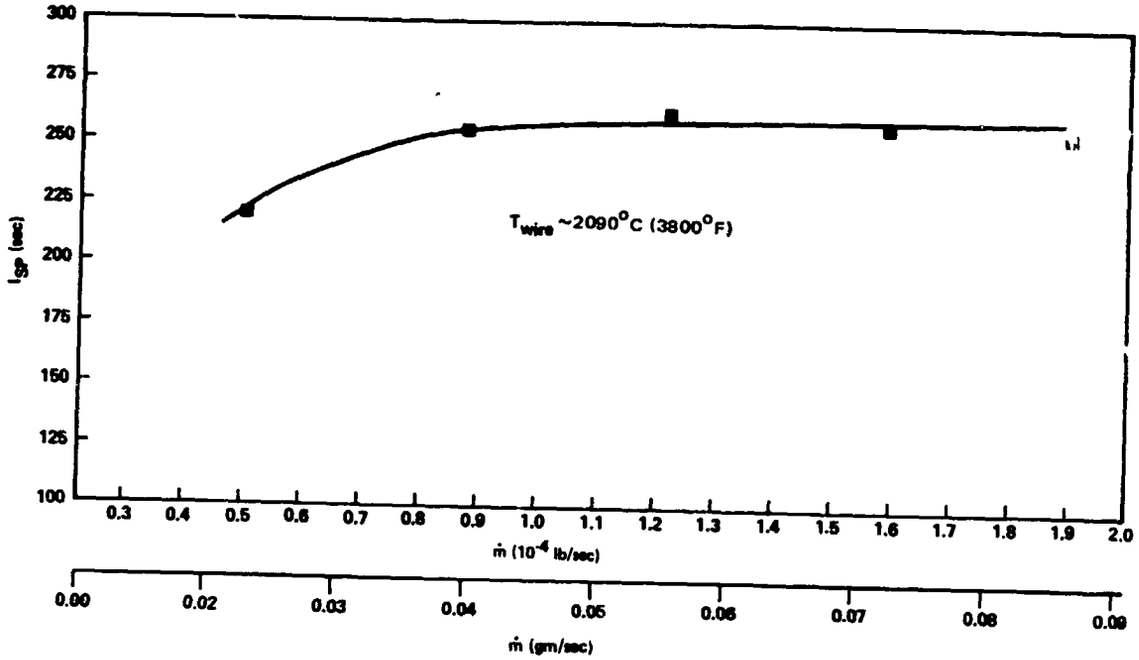


(b)

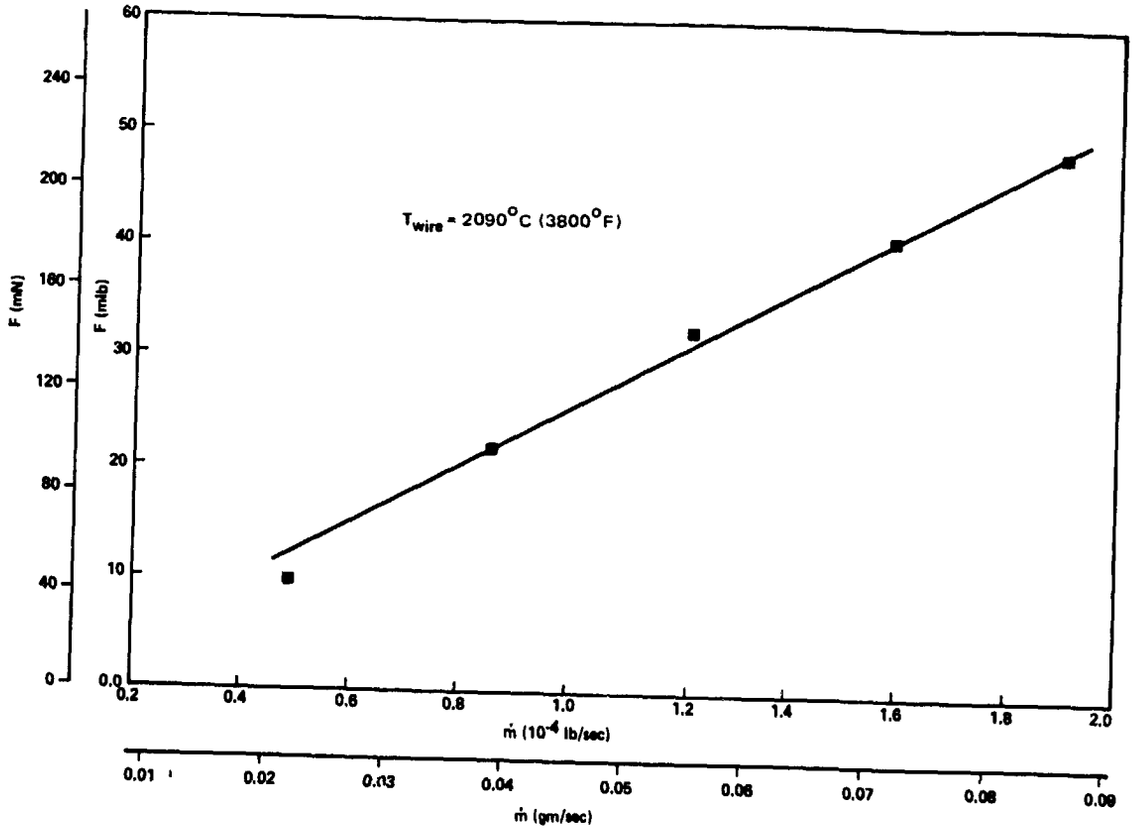


(c)

Figure 23. Performance Versus Mass Flow, Ammonia Propellant, ~2090°C (3800°F) Heater Temperature (Continued)

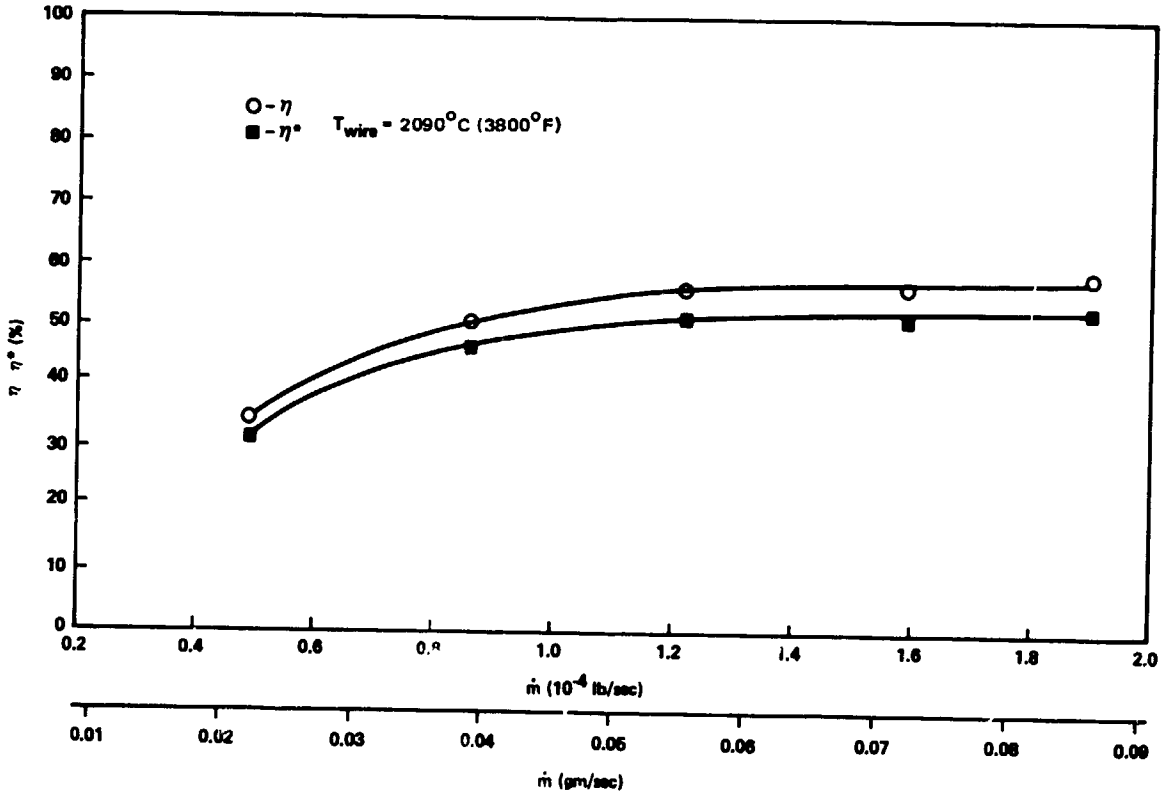


(d)

Figure 23. Performance Versus Mass Flow, Ammonia Propellant, ∿2090°C (3800°F) Heater Temperature (Continued)

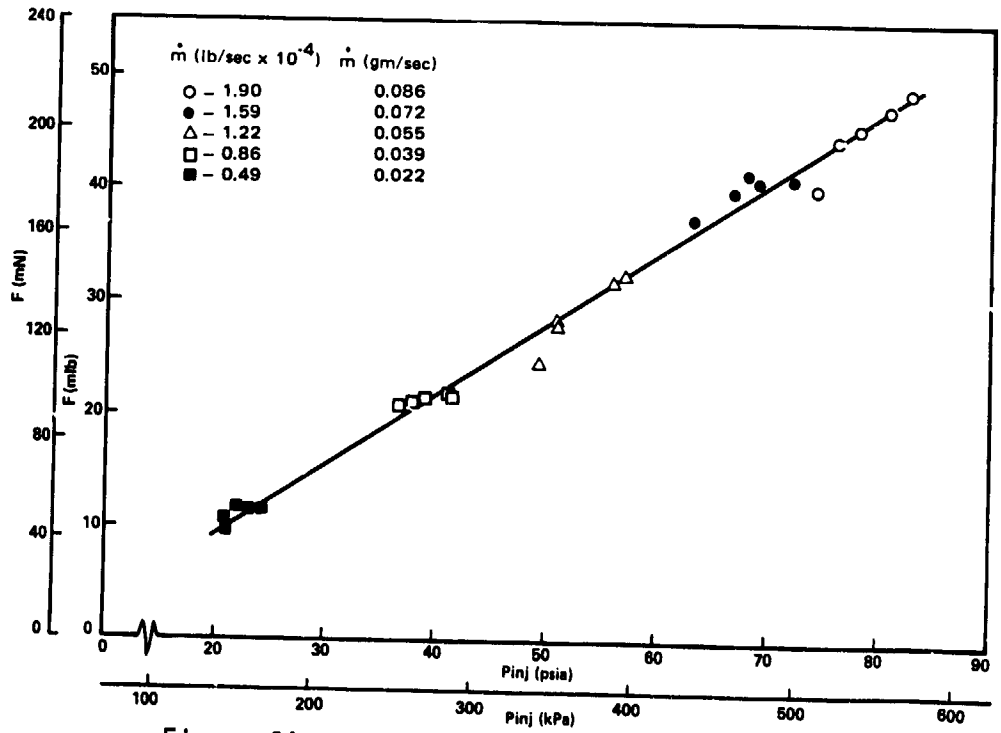


Figure 24. Thrust Versus Injection Pressure, Ammonia Propellant

## 5. POST-TEST ANALYSIS

The first thruster test unit, serial number 212, exhibited an increase in heater element resistance upon completion of its nitrogen test series. This test unit was then subjected to post-test analysis as discussed below. Hydrogen and ammonia tests were conducted with the second thruster test unit, serial number 229. It was in good condition upon conclusion of the hydrogen and ammonia tests.

Thruster test unit 212 was cut open to examine its heater element. Scanning electron microscope (SEM) photographs of the heater element are shown in Figure 25 at various magnifications. Contamination of the element wire at its upper support post is seen in Figure 25a. Less contamination is seen near the lower support in 25b. Figures 25c and 25d show the upper post at higher magnification. Closeups in 25e and 25f show different surface morphology at the right and left corners of the post, respectively.

Wavelength dispersive X-ray analysis of the contaminated heater element from thruster 212 showed that the heater was heavily oxidized. Qualitative estimates of the elements detected showed high tungsten intensity, with low intensity for rhenium, oxygen, and carbon. The heater was extremely brittle, as evidenced by the fact that it shattered into several pieces while being removed from the SEM following dispersive analysis.

Ion microprobe mass analysis (IMA) of the heater element surface from thruster 212 showed tungsten and tungsten oxides predominantly. The IMA thereby confirmed the wavelength dispersive x-ray analysis of this surface. It was concluded that the contaminant on the heater wire was tungsten oxide, probably from water vapor in the nitrogen gas supply.

Additional SEM photographs were taken of the wire cross sections as shown in Figure 26. Examination of the cross section shows three zones (labeled 1, 2, and 3 in Figure 26a) which have different surface morphology. It was speculated that the wire may have been partially fractured, and was only conducting electricity through zone 3 prior to its final break. This would help explain the high wire resistance seen after testing. In order to

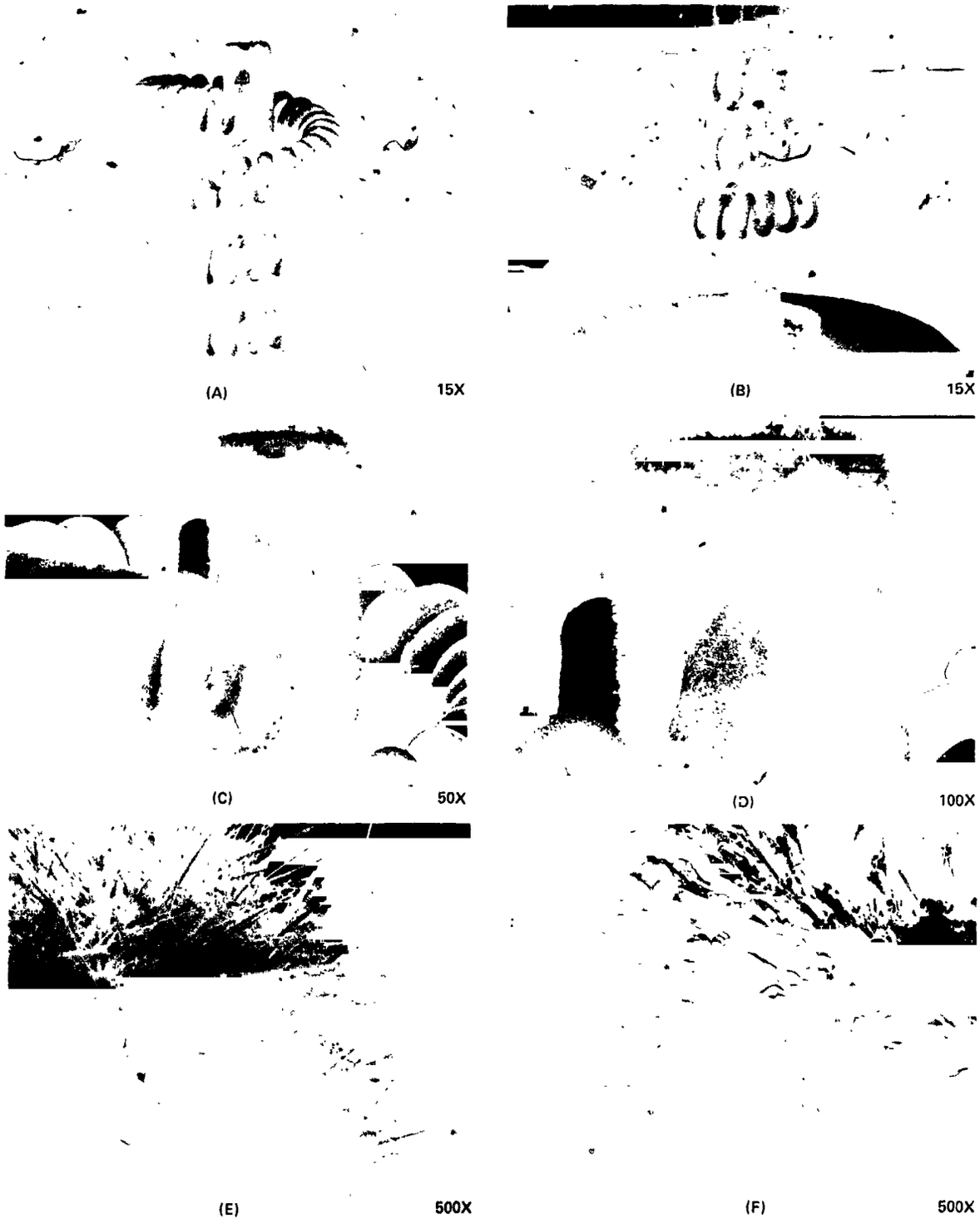


Figure 25. SEM Photographs, Thruster 212 Heater Element, After Nitrogen Characterization Tests

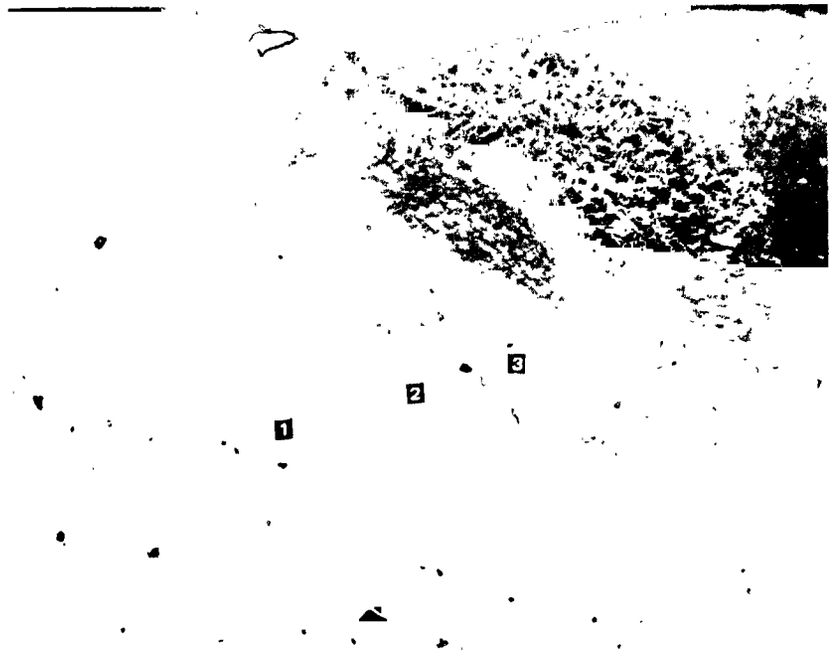


(a) 300X

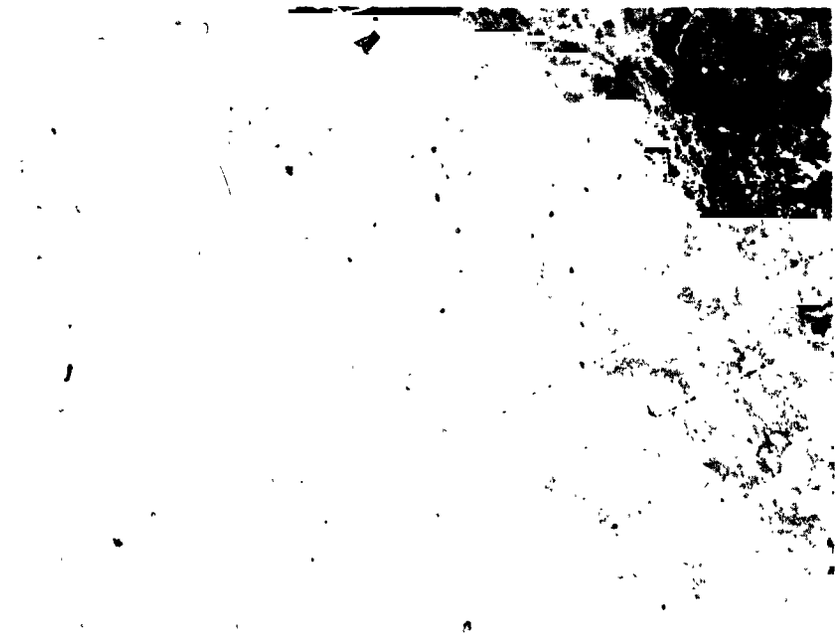

(b) 1000X

Figure 26. SEM Photographs, Thruster 212 Heater Element Cross Section, After Nitrogen Characterization Tests

continue this investigation, oxygen peak-to-background readings were taken with the x-ray analyzer in each of the three zones. These readings showed relative intensities of 15, 31, and 53 for zones 1, 2, and 3, respectively. This led to the conclusion that zone 1 (shown close-up in Figure 26b) was a clean break in the tungsten wire, that zone 2 was lightly oxidized, and that surface zone 3 was heavily oxidized. Zone 2 was probably exposed to the oxidizing environment during testing, which implies that the wire was conducting primarily through zone 3.

## 6. DISCUSSION OF RESULTS

With nitrogen propellant, the thruster test unit exhibited 73 ±13.9 percent ($2\sigma$) overall efficiency over a 2.28:1 mass flow range. At its design point, the Vela thruster (Reference 4) yielded 82 percent overall efficiency. The latter thruster was rated at 123 seconds $I_{sp}$. Its design incorporated a heated core wound flow tube operating at 540°C (1000°F). The thruster test unit on this project was operated up to 169 seconds $I_{sp}$ (see Figure 13) with nitrogen.

Table 2 compares the thruster test unit performance with hydrogen propellant to other hydrogen resistojets. Its efficiency compares favorably with other thrusters in the same size range. Its specific impulse, however, is low because it has insufficient heat exchange area to raise the exhaust gas temperature high enough to deliver more $I_{sp}$. Two methods may be employed to increase specific impulse: (1) put a preheater on the gas inlet line to the heat exchanger, (2) redesign the heat exchanger specifically for hydrogen propellant.*

Table 3 compares the thruster test unit performance with other ammonia resistojets. Again, its efficiency compares favorably but its specific impulse is lower than the other thrusters.

The overall efficiency of an electrothermal thruster, as defined by equation (2), is more commonly expressed as

$$\eta^* = \frac{F^2}{2\dot{m}P_{in}} = \frac{F\,I_{sp}}{2(IV + \dot{m}\,h)} \qquad (7)$$

*Recall that the heat exchanger was originally designed for hot gas, hydrazine propellant inlet.

Table 2. Performance Comparison with Other Hydrogen Resistojets

| | | | | | | |
|---|---|---|---|---|---|---|
| Input Power, kW | 0.2 | 0.5 | 1.0 | 3.0 | 3.0 | 30.0 |
| Propellant | $H_2$ | $H_2$ | $H_2$ | $H_2$ | $H_2$ | $H_2$ |
| Heater Configuration | Concentric Tubes | Double Helix | Concentric Contact | Concentric Tubes | Transverse Coils | Concentric Contact |
| Specific Impulse, sec | 670 | 550 | 729 | 840 | 838 | 846 |
| Overall Efficiency | 0.59 | 0.61 | | | | |
| Electrical Efficiency | 0.69 | 0.73 | 0.63 | 0.88 | 0.74 | 0.85 |
| Laboratory | Marquardt | TRW | Giannini | Marquardt | AVCO | Giannini |

Sources: References 1, 10, 11 and 12

Table 3. Performance Comparison with Other Ammonia Resistojets

| | | | |
|---|---|---|---|
| Input Power, kW | 0.2 | 0.5 | 12.3 |
| Propellant | $NH_3$ | $NH_3$ | $NH_3$ |
| Heater Configuration | Concentric Tubes | Double Helix | Concentric Contact |
| Specific Impulse, sec | 320 | 255 | 423 |
| Overall Efficiency | 0.45 | 0.52 | 0.50 |
| Electrical Efficiency | 0.51 | 0.57 | |
| Laboratory | Marquardt | TRW | Giannini |

Sources: References 1 and 11

which is derived from the ratio of jet power to total input power. This ratio may be further broken down as

$$\eta^* = \frac{P_j}{P_n} \cdot \frac{P_n}{P_p} \cdot \frac{P_p}{P_{in}} \tag{8}$$

where the first term is the ratio of jet power to the power remaining in the flow at the nozzle exit, the second term is the ratio of the exit nozzle power to the power transferred to the propellant, and the third term is the ratio of propellant power to total power input. The first term is a flow efficiency, containing frozen flow losses and any thermal energy remaining in the flow from incomplete expansion to infinity. The second term is a nozzle efficiency, and the third term is a thermal efficiency (propellant heater efficiency). Accordingly, equation (8) becomes

$$\eta^* = \eta_f (\eta_n)^2 \eta_{th} \tag{9}$$

where

$\eta_f$ = flow efficiency,

$\eta_n$ = nozzle efficiency,

$\eta_{th}$ = thermal efficiency.

The reason $\eta_n$ appears as a square term in equation (9) is because it is usually expressed as an aerodynamic efficiency, i.e., the ratio of delivered to ideal specific impulse. The relationship between nozzle power efficiency and aerodynamic efficiency is

$$(\eta_n)^2 = \frac{P_n}{P_p} = \frac{h_n}{h_p} = \left[\frac{(I_{sp})_n}{(I_{sp})_p}\right]^2 \tag{10}$$

where $\eta$, P, h, and $I_{sp}$ are efficiency, power, enthalpy, and specific impulse, respectively, and the subscripts n and p denote nozzle and propellant, respectively.

With nitrogen propellant, the throat Reynolds number was approximately 11,000 at the maximum mass flow rate tested. Assuming a nozzle efficiency >0.95 for this condition, $(\eta_n)^2 = 0.90$. At the nozzle expansion ratio of 200, $\eta_f \cong 0.91$. Thus,

$$\eta_{th} = \frac{\eta^*}{\eta_f (\eta_n)^2} = \frac{0.73}{0.91(0.90)} = 0.89 \qquad (11)$$

with nitrogen propellant. This compares favorably with efficiency for hydrazine discussed earlier in Section 2.

With hydrogen propellant, the throat Reynolds number was approximately 4500 at the maximum flow rate tested. From the data in Reference 9, the nozzle efficiency is estimated at 0.92, yielding $(\eta_n)^2 = 0.85$. At $\varepsilon = 200$, $\eta_f \cong 0.92$. Then

$$\eta_{th} = \frac{0.61}{0.92(0.85)} = 0.78 \qquad (12)$$

with hydrogen propellant. This analysis indicates that a more efficient heat exchanger could be designed for hydrogen molecular species.

With ammonia propellant, the throat Reynolds number was approximately 8000 at the maximum flow rate tested. Assuming nozzle efficiency >0.95, $(\eta_n)^2 = 0.90$ At $\alpha = 0.4$, $\eta_f = 0.64$. Thus,

$$\eta_{th} = \frac{0.515}{0.64(0.90)} = 0.89 \qquad (13)$$

with ammonia propellant, which also agrees favorably with hydrazine results.

The thermal efficiency calculations presented above tend to confirm the inferences drawn earlier from comparisons with other resistojets. It is therefore recommended that further development work to improve vortex

heat exchanger performance concentrate specifically on heat exchanger design for hydrogen propellant to optimize its overall efficiency for this particular propellant.

Another recommendation for increasing specific impulse is to develop a preheater for the vortex heat exchanger. Conceptually, a simple heated tube coil, having the geometry defined by Figure 27, was investigated. At typical flow rates, to raise propellant gas temperatures from 25°C (80°F) to 1090°C (2000°F) in the preheater coil would require 275 watts for nitrogen, 360 watts for hydrogen, and 520 watts for ammonia ($\alpha$ = 1). Using a design criteria of 32 watts/cm$^2$ (5 watts/in$^2$) power density, the coil dimensions listed in Table 4 are obtained. Further diagnostic development with preheaters having these, or similar, dimensions will yield data at higher propellant gas temperatures in the vortex heat exchanger and will result in higher specific impulse performance.

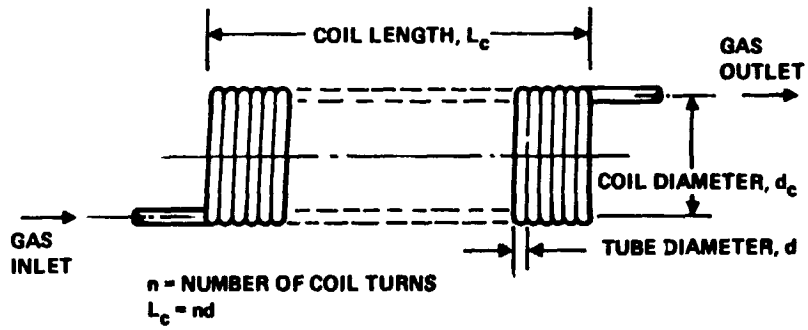


Figure 27. Conceptual Preheater Coil Geometry

Table 4. Conceptual Preheater Coil Dimensions

| Propellant | Tube Diameter d cm (inches) | Coil Diameter $d_c$ cm (inches) | Coil Length $L_c$ cm (inches) | Number of Coil Turns n |
|---|---|---|---|---|
| Nitrogen | 0.32 (0.125) | 2.5 (1.0) | 14 (5.5) | 44 |
| Hydrogen | 0.32 (0.125) | 2.5 (1.0) | 17 (7.3) | 58 |
| Ammonia | 0.32 (0.125) | 5.1 (2.0) | 19 (5.3) | 42 |

# 7. CONCLUSIONS

The flight-qualified HiPEHT demonstrated its adaptability to a variety of propellants. Originally qualified with hot hydrazine decomposition products entering its augmentation heat exchanger, the thruster was operated with cold gas propellant inlet to the heat exchanger. It was run with nitrogen, hydrogen, and ammonia propellants.

The vortex heat exchanger exhibited good overall efficiency with all the propellants employed: hydrazine, nitrogen, hydrogen, and ammonia. Efficiency comparisons with other resistojet thrusters, employing a number of different heating techniques, were made. These comparisons showed that the vortex heat exchanger can be efficiently operated with a number of different propellants.

The specific impulse delivered by the vortex heat exchanger will be higher than reported herein when the heat exchanger is operated with hot propellant inlet gases. Conceptual design of a preheater for this purpose is presented in Section 6. At low flow rates, the heat exchanger is not as efficient. At high flow rates, it does not have sufficient heat exchange area, with cold gas inlet, to raise the exhaust gas temperature high enough to deliver specific impulse closer to theoretical limits.

Contamination control is particularly important with immersed high temperature heating elements. Evidence of nitrogen propellant contamination, probably by water vapor, was seen on this project in the form of tungsten oxides which were present on the thruster heating element following the nitrogen test series.

## REFERENCES


1. Jahn, R.G.. Physics of Electric Propulsion, Chapter 6, McGraw-Hill, New York, 1968.

2. Page, R.J. and Short, R.A., "Advanced Resistojet Propulsion and Control Systems for Spacecraft," ASME 70-Av/SpT-10, June 1970.

3. Jack, J.R., "Theoretical Performance of Propellants Suitable for Electrothermal Jet Engines," ARS Journal, December 1961, pp. 1685-1689.

4. Jackson, F.A., et al, "An Operational Electrothermal Propulsion System for Spacecraft Reaction Control," AIAA Paper 66-213, March 1966.

5. Dressler, G.A., et al, "Flight Qualification of the Augmented Electrothermal Hydrazine Thruster," AIAA Paper 81-1410, July 1981.

6. Petrash, D.A., "Station Keeping Will Eat Energy on a New Scale," Astronautics and Aeronautics, Vol. 21, No. 3, March 1983, pp. 64-65.

7. Murch, C.K., and Krieve, W.F., "Electrothermal Thruster Performance with Biowaste Propellants," AIAA 70-1161, September 1970.

8. Pugmire, T.K., et al, "Applied Resistojet Technology," AIAA 70-211, January 1970.

9. Murch, C.K., et al, "Performance Losses in Low-Reynolds-Number Nozzles," Journal of Spacecraft and Rockets, Vol. 5, No. 9, September 1968, pp. 1090-1094.

10. Yoshida, R.Y., Halbach, C.R., and Hill, C.S., "Life Test Summary and High-Vacuum Tests of 10-mlb Resistojets," Journal of Spacecraft and Rockets, Vol. 8, No. 4, April 1971, pp. 414-416.

11. Ducati, A.C., Muehlberger, E., and Todd, J.P., "Resistance-Heated Thrustor Research," AFAPL-TR-65-71, July 1965.

12. Page, R.J., et al, "3-kw Concentric Tubular Resistojet Performance," Journal of Spacecraft and Rockets, Vol. 3, 1966, p. 1669.

# APPENDIX A
## HiPEHT PERFORMANCE

Thruster performance as a function of flow rate is presented in Figure A-1, where thrust, specific impulse, vortex heat exchanger power, and vortex heater element temperature data from 16 thrusters have been summarized. The $\pm 2\sigma$ envelopes given in each case include data dispersions because of both instrumentation and unit-to-unit variations. Figure A-2 is a graph showing specific impulse as a function of heater element temperature. Wire temperatures as high as 4400°F, yielding specific impulses to 320 seconds, have been achieved. In practice, element temperatures have been limited to about 3800°F to afford design margin.

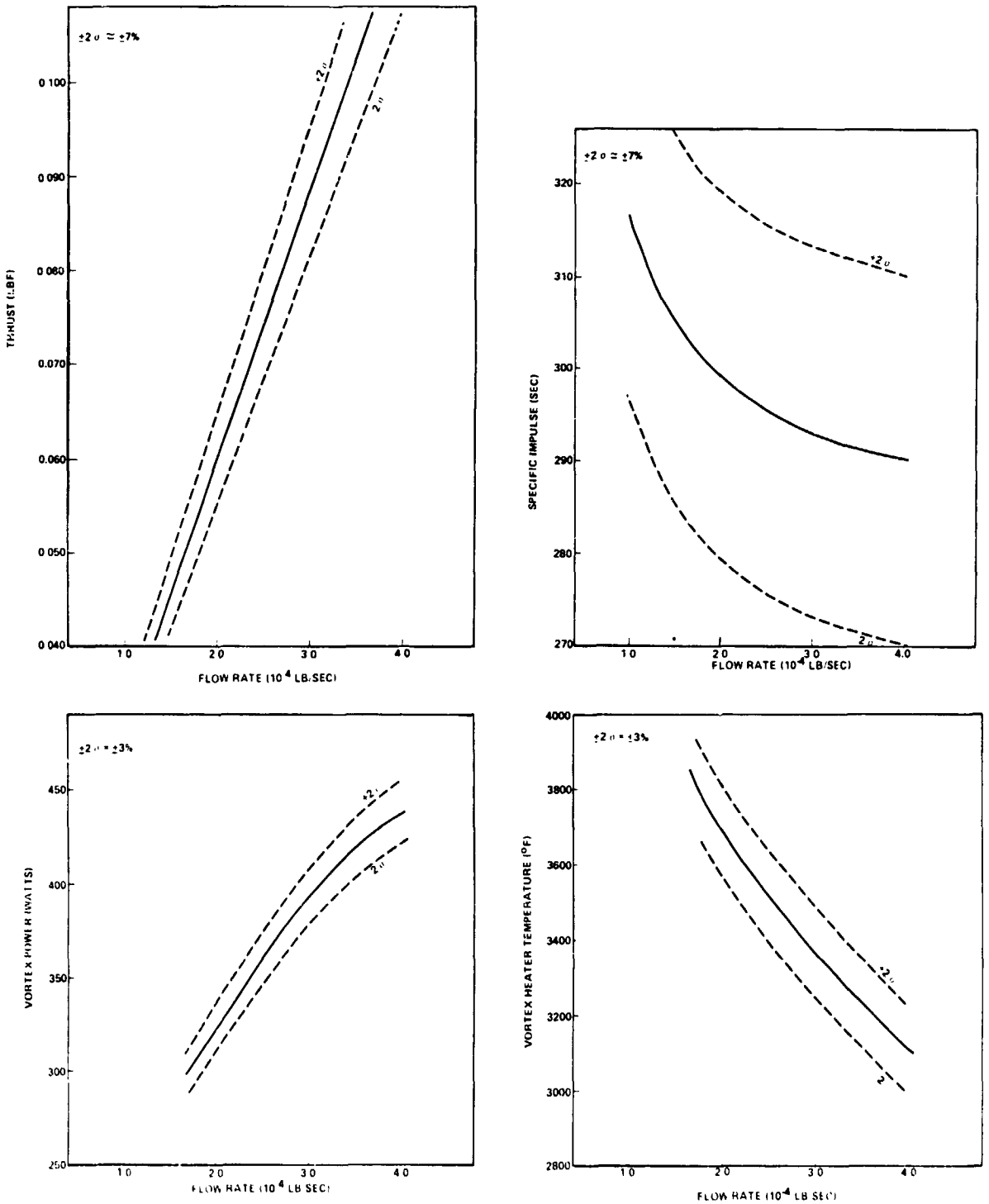


Figure A-1. Thruster Performance Versus FLow Rate with Hydrazine Propellant

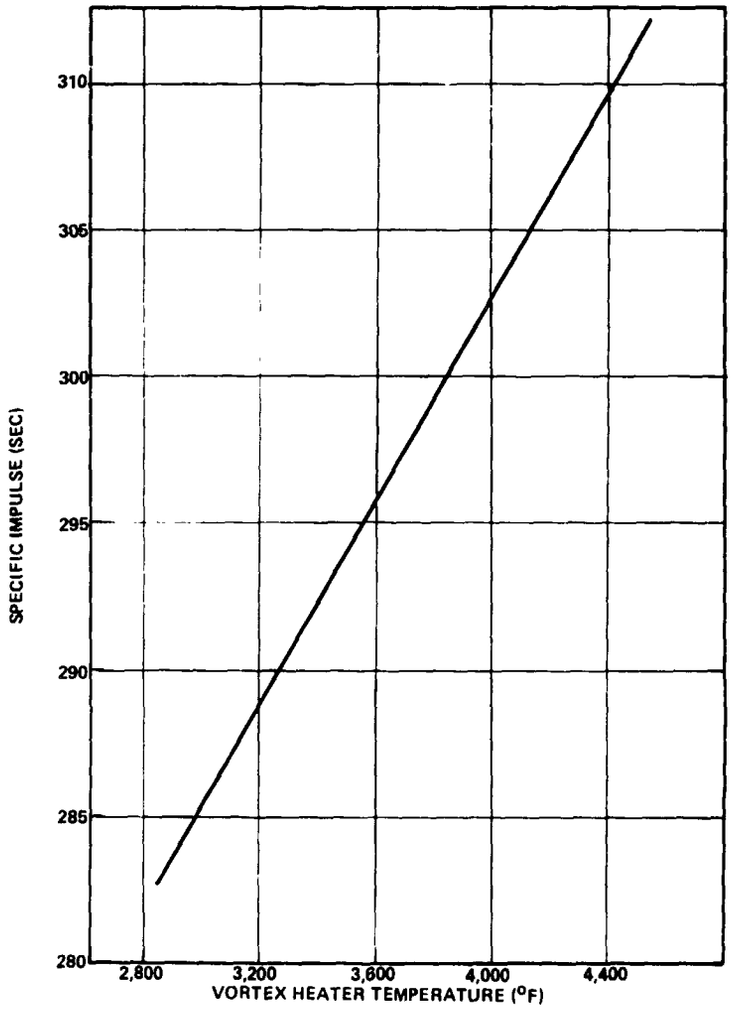


Figure A-2. Delivered Specific Impulse Versus Vortex Heater Element Temperature with Hydrazine Propellant

# APPENDIX B

# NITROGEN DATA SUMMARY

## NITROGEN DATA SUMMARY

| Test No. | 1R | 2R | 3R | 4R | 5R | 6 | 7 | 8 | 8R | 8R2 | 8R3 | 9 | 9R | 9R2 | 10 |
|---|---|---|---|---|---|---|---|---|---|---|---|---|---|---|---|
| $\dot{m}$ (lb/sec x $10^{-4}$) | 2.85 | 2.32 | 1.78 | 1.27 | 0.71 | 2.85 | 2.85 | 2.85 | 2.85 | 2.85 | 2.85 | 2.85 | 2.85 | 2.85 | 2.85 |
| $T_{wire}$ ($^{o}$F) | | | | | | 3000 | 3200 | 3400 | 3400 | 3400 | 3400 | 3600 | 3600 | 3600 | 3800 |
| $P_{inj}$ (psia) | 44 | 36 | 28 | 20 | 11 | 82 | 84 | 86 | 90 | 86 | 81 | 88 | 93 | 87 | 95 |
| F (mlb) | 21.2 | 17.2 | 13.6 | 9.7 | 6.2 | 41.6 | 42.5 | 43.4 | 46.6 | 43.6 | 41.5 | 48.2 | 46.7 | 44.4 | 47.2 |
| $I_{sp}$ (sec) | 74 | 74 | 76 | 77 | 88 | 146 | 149 | 152 | 164 | 153 | 146 | 169 | 164 | 156 | 166 |
| P (watts) | | | | | | 145 | 156 | 170 | 163 | 144 | 123 | 183 | 183 | 151 | 187 |
| $\eta$ (%) | | | | | | 91.4 | 88.2 | 84.7 | 101.7 | 101.0 | 107.3 | 97.2 | 91.4 | 99.8 | 90.9 |
| $\eta^*$ (%) | | | | | | 71.8 | 70.4 | 68.7 | 81.9 | 79.2 | 81.2 | 79.9 | 75.2 | 79.1 | 75.1 |

| Test No. | 10R | 11 | 12 | 13 | 13R | 14 | 14R | 15 | 15R | 16 | 17 | 18 | 18R | 19 | 20 |
|---|---|---|---|---|---|---|---|---|---|---|---|---|---|---|---|
| $\dot{m}$ (lb/sec x $10^{-4}$) | 2.85 | 2.32 | 2.32 | 2.32 | 2.32 | 2.32 | 2.32 | 2.32 | 2.32 | 1.71 | 1.71 | 1.71 | 1.71 | 1.71 | 1.71 |
| $T_{wire}$ ($^{o}$F) | 3800 | 3000 | 3200 | 3400 | 3400 | 3600 | 3600 | 3800 | 3800 | 3000 | 3200 | 3400 | 3400 | 3600 | 3800 |
| $P_{inj}$ (psia) | 88 | 66 | 68 | 70 | 68 | 70 | 69 | 71 | 69 | 50 | 52 | 57 | 50 | 58 | 60 |
| F (mlb) | 45.1 | 33.0 | 33.7 | 34.7 | 37.6 | 34.9 | 35.0 | 35.1 | 35.1 | 24.8 | 25.4 | 27.6 | 25.7 | 27.8 | 29.0 |
| $I_{sp}$ (sec) | 158 | 142 | 145 | 150 | 162 | 150 | 151 | 151 | 151 | 139 | 143 | 155 | 144 | 156 | 163 |
| P (watts) | 159 | 113 | 125 | 139 | 109 | 144 | 116 | 154 | 117 | 85 | 96 | 105 | 75 | 114 | 124 |
| $\eta$ ( ) | 98.9 | 90.6 | 85.3 | 81.6 | 121.4 | 79.4 | 99.4 | 75.3 | 98.8 | 88.5 | 82.3 | 89.3 | 107.9 | 83.2 | 83.3 |
| $\eta^*$ ( ) | 78.5 | 70.5 | 67.8 | 66.3 | 93.8 | 64.9 | 77.8 | 62.3 | 77.4 | 68.6 | 65.4 | 72.2 | 81.2 | 68.3 | 69.4 |

NITROGEN DATA SUMMARY (Continued)

| Test No. | 21 | 22 | 23 | 23R | 24 | 25 | 26 | 27 | 28 | 29 | 30 |
|---|---|---|---|---|---|---|---|---|---|---|---|
| $\dot{m}$ (lb/sec x $10^{-4}$) | 1.25 | 1.25 | 1.25 | 1.25 | 1.25 | 1.25 | 0.71 | 0.71 | 0.71 | 0.71 | 0.71 |
| $T_{wire}$ ($^{o}$F) | 3000 | 3200 | 3400 | 3400 | 3600 | 3800 | 3000 | 3200 | 3400 | 3600 | 3800 |
| $P_{inj}$ (psia) | 38 | 39 | 40 | 35 | 41 | — | 30 | 31 | 31 | 31 | 32 |
| F (mlb) | 17.6 | 18.2 | 19.6 | 17.8 | 19.2 | 19.6 | 9.7 | 9.9 | 10.1 | 10.2 | 10.4 |
| $I_{sp}$ (sec) | 141 | 146 | 157 | 142 | 153 | 157 | 137 | 140 | 143 | 144 | 146 |
| P (watts) | 61 | 68 | 75 | 54 | 82 | 90 | 36 | 42 | 46 | 51 | 57 |
| $\eta$ (%) | 89.3 | 85.6 | 89.1 | 102.8 | 78.2 | 74.5 | 80.9 | 71.9 | 68.5 | 62.6 | 58.2 |
| $\eta^*$ (%) | 69.4 | 68.1 | 72.4 | 77.8 | 64.6 | 62.5 | 63.5 | 58.3 | 56.4 | 52.5 | 49.7 |

# APPENDIX C

# HYDROGEN DATA SUMMARY

## HYDROGEN DATA SUMMARY

| Test No. | 31R | 32R | 33R | 34R | 35R | 36R | 37 | 38 | 39 | 40 | 41 | 42R | 43 | 44 | 45 |
|---|---|---|---|---|---|---|---|---|---|---|---|---|---|---|---|
| $\dot{m}$ (lb/sec x $10^{-4}$) | 0.60 | 0.49 | 0.38 | 0.26 | 0.15 | 0.60 | 0.60 | 0.60 | 0.60 | 0.60 | 0.49 | 0.49 | 0.49 | 0.49 | 0.49 |
| $T_{wire}$ ($^{o}$F) | | | | | | 3000 | 3200 | 3400 | 3600 | 3800 | 3000 | 3200 | 3400 | 3600 | 3800 |
| $P_{inj}$ (psia) | 51 | 45 | 38 | 32 | 25 | 59 | 61 | 62 | 64 | 65 | 48 | 49 | 51 | 52 | 53 |
| F (mlb) | 15.0 | 12.7 | 9.5 | 6.6 | 3.5 | 30.7 | 31.3 | 31.9 | 32.6 | 33.2 | 24.3 | 25.0 | 25.6 | 26.5 | 27.1 |
| $I_{sp}$ (sec) | 250 | 259 | 250 | 254 | 233 | 512 | 522 | 532 | 543 | 553 | 496 | 511 | 523 | 541 | 553 |
| P (watts) | | | | | | 404 | 434 | 465 | 496 | 534 | 318 | 344 | 373 | 404 | 434 |
| $\eta$ ( ) | | | | | | 84.7 | 82.0 | 79.5 | 77.8 | 75.1 | 82.5 | 81.0 | 78.2 | 77.4 | 75.3 |
| $\eta^{*}$ ( ) | | | | | | 66.2 | 65.0 | 63.9 | 63.4 | 61.9 | 63.9 | 63.8 | 62.7 | 62.9 | 62.1 |

| Test No. | 46 | 47 | 48 | 49 | 50 | 51 | 52 | 53 | 54 | 55 | 56 | 57 | 58 | 59 | 60 |
|---|---|---|---|---|---|---|---|---|---|---|---|---|---|---|---|
| $\dot{m}$ (lb/sec x $10^{-4}$) | 0.38 | 0.38 | 0.38 | 0.38 | 0.38 | 0.26 | 0.26 | 0.26 | 0.26 | 0.26 | 0.15 | 0.15 | 0.15 | 0.15 | 0.15 |
| $T_{wire}$ ($^{o}$F) | 3000 | 3200 | 3400 | 3600 | 3800 | 3000 | 3200 | 3400 | 3600 | 3800 | 3000 | 3200 | 3400 | 3600 | 3800 |
| $P_{inj}$ (psia) | 38 | 39 | 40 | 41 | 42 | 27 | 28 | 28 | 29 | 30 | 18 | 18 | 19 | 20 | 21 |
| F (mlb) | 18.2 | 18.6 | 19.3 | 19.9 | 20.7 | 11.9 | 12.1 | 12.3 | 12.9 | 13.2 | 6.5 | 6.6 | 6.7 | 6.8 | 7.0 |
| $I_{sp}$ (sec) | 483 | 490 | 509 | 523 | 545 | 457 | 465 | 473 | 498 | 509 | 432 | 438 | 446 | 453 | 466 |
| P (watts) | 242 | 263 | 285 | 307 | 329 | 156 | 166 | 178 | 195 | 216 | 99 | 112 | 126 | 144 | 162 |
| $\eta$ ( ) | 79.2 | 75.4 | 75.1 | 73.9 | 74.7 | 75.9 | 73.8 | 71.4 | 71.6 | 67.8 | 61.7 | 56.4 | 51.5 | 46.6 | 44.0 |
| $\eta^{*}$ ( ) | 61.1 | 59.3 | 60.0 | 59.9 | 61.3 | 57.7 | 56.9 | 55.9 | 57.2 | 55.3 | 48.0 | 45.0 | 42.0 | 39.0 | 37.4 |

# APPENDIX D

# AMMONIA DATA SUMMARY

## AMMONIA DATA SUMMARY

| Test No. | 61 | 62 | 63 | 64 | 65 | 66 | 67 | 68 | 69 | 70 | 71 | 72 | 73 | 74 | 75 |
|---|---|---|---|---|---|---|---|---|---|---|---|---|---|---|---|
| $\dot{m}$ (lb/sec x $10^{-4}$) | 1.90 | 1.59 | 1.22 | 0.86 | 0.49 | 1.90 | 1.90 | 1.90 | 1.90 | 1.90 | 1.59 | 1.59 | 1.59 | 1.59 | 1.59 |
| $T_{wire}$ ($^{o}$F) | | | | | | 3000 | 3200 | 3400 | 3600 | 3800 | 3000 | 3200 | 3400 | 3600 | 3800 |
| $P_{inj}$ (psia) | 38 | 32 | 24 | 18 | 10 | 74 | 76 | 78 | 81 | 83 | 63 | 67 | 68 | 69 | 72 |
| F (mlb) | 20.8 | 17.4 | 13.2 | 9.5 | 5.0 | 39.9 | 44.5 | 45.4 | 47.3 | 48.7 | 37.4 | 39.7 | 41.5 | 40.8 | 41.1 |
| $I_{sp}$ (sec) | 110 | 109 | 108 | 110 | 102 | 210 | 234 | 239 | 249 | 257 | 235 | 250 | 251 | 257 | 259 |
| P (watts) | | | | | | 340 | 372 | 404 | 435 | 466 | 293 | 329 | 356 | 379 | 415 |
| $\eta$ (%) | | | | | | 53.7 | 61.6 | 58.5 | 59.0 | 58.5 | 65.5 | 67.7 | 63.9 | 60.3 | 55.9 |
| $\eta^*$ (%) | | | | | | 46.8 | 53.8 | 52.0 | 52.9 | 52.8 | 57.2 | 58.2 | 57.1 | 54.3 | 50.8 |

| Test No. | 76 | 77 | 78 | 79 | 80 | 81 | 82 | 83 | 84 | 85 | 86 | 87 | 88 | 89 | 90 |
|---|---|---|---|---|---|---|---|---|---|---|---|---|---|---|---|
| $\dot{m}$ (lb/sec x $10^{-4}$) | 1.22 | 1.22 | 1.22 | 1.22 | 1.22 | 0.86 | 0.86 | 0.86 | 0.86 | 0.86 | 0.49 | 0.49 | 0.49 | 0.49 | 0.49 |
| $T_{wire}$ ($^{o}$F) | 3000 | 3200 | 3400 | 3600 | 3800 | 3000 | 3200 | 3400 | 3600 | 3800 | 3000 | 3200 | 3400 | 3600 | 3800 |
| $P_{inj}$ (psia) | 49 | 51 | 51 | 56 | 57 | 37 | 38 | 39 | 41 | 41 | 21 | 21 | 22 | 23 | 24 |
| F (mlb) | 24.6 | 28.6 | 28.6 | 31.8 | 32.3 | 20.7 | 21.0 | 21.3 | 22.0 | 22.0 | 9.8 | 10.3 | 10.5 | 10.7 | 10.7 |
| $I_{sp}$ (sec) | 202 | 235 | 235 | 260 | 264 | 241 | 244 | 248 | 256 | 256 | 199 | 210 | 215 | 219 | 219 |
| P (watts) | 233 | 255 | 272 | 309 | 331 | 180 | 195 | 211 | 227 | 243 | 99 | 108 | 120 | 135 | 151 |
| $\eta$ (%) | 46.5 | 57.5 | 53.8 | 58.4 | 56.2 | 60.3 | 57.4 | 54.7 | 54.1 | 50.5 | 42.9 | 43.7 | 40.8 | 37.8 | 33.8 |
| $\eta^*$ (%) | 40.8 | 51.0 | 48.1 | 52.9 | 51.2 | 53.5 | 51.4 | 49.3 | 49.1 | 46.2 | 37.9 | 39.0 | 36.8 | 34.5 | 31.1 |

# APPENDIX E

## NOMENCLATURE

| | |
|---|---|
| $d$ | Tube diameter, centimeters |
| $d_c$ | Coil diameter, centimeters |
| $F$ | Thrust, Newtons (mlbf in Equations 1-4) |
| $h$ | Enthalpy, Joules/gram |
| $h_p$ | Propellant enthalpy, Joules/gram |
| $h_n$ | Nozzle enthalpy, Joules/gram |
| $I$ | Current, amperes |
| $I_{sp}$ | Specific impulse, seconds |
| $(I_{sp})_n$ | Delivered specific impulse, seconds |
| $(I_{sp})_p$ | Ideal specific impulse, seconds |
| $L_c$ | Coil length, centimeters |
| $\dot{m}$ | Mass flow, grams/second |
| $n$ | Number of coil turns |
| $P$ | Electrical input power, watts |
| $P_{in}$ | Input power, watts |
| $P_j$ | Jet power, watts |
| $P_n$ | Nozzle power, watts |
| $P_p$ | Propellant power, watts |
| $P_{inj}$ | Injection pressure, kiloPascals |
| $T_{wire}$ | Heater element wire temperature, degrees |
| $V$ | Voltage, volts |
| $\alpha$ | Dissociation fraction |
| $\epsilon$ | Expansion ratio |
| $\eta$ | Electrical efficiency |

NOMENCLATURE (Continued)

| | |
|---|---|
| $\eta_f$ | Flow efficiency |
| $\eta_n$ | Nozzle efficiency |
| $\eta_{th}$ | Thermal efficiency |
| $\eta^*$ | Overall efficiency |
| $\sigma$ | Standard deviation |